Parametric study on the integrity of wellbores in CO2 storage sites

Bagheri, M., Shariatipour, S. M. & Ganjian, E.

Original citation & hyperlink:
Bagheri, M, Shariatipour, SM & Ganjian, E 2021, 'Parametric study on the integrity of wellbores in CO2 storage sites', Construction and Building Materials, vol. 268, 121060.
https://dx.doi.org/10.1016/j.conbuildmat.2020.121060

DOI 10.1016/j.conbuildmat.2020.121060
ISSN 0950-0618

Publisher: Elsevier

Parametric study on the integrity of wellbores in CO_2 storage sites

Mohammadreza Bagheri[a,*], Seyed M. Shariatipour[a], Eshmaiel Ganjian[b]

[a] Research Centre for Fluid and Complex Systems, Coventry University, Mile Lane, Coventry CV1 2NL, UK

[b] School of Energy, Construction and Environment, Built & Natural Environment Research Centre, Coventry University, Coventry CV1 5FB, UK

[*] Corresponding author, *E-mail address:* bagherim@coventry.ac.uk

Abstract

Carbon capture and storage is considered as an amelioration technique to address the increasing level of carbon dioxide in the atmosphere. Depleted oil and gas reservoirs are potential candidates for the long sequestration of the captured carbon dioxide. The huge number of drilled oil and gas wells in these hydrocarbon reservoirs around the world, however, pose a threat to the integrity of geological CO_2 storage projects. These wells are direct connections to the Earth's surface and even when capped, any defects in their structure can become high leakage pathways. To predict the consequences of this possible loss, a model was developed and introduced by the authors based on coupling the geochemical and geomechanical alterations benefitting from a plastic-damage model. This model simulates the alteration of the rock-cement-casing assemblage in abandoned wells for carbon storage sites. In this paper, a parametric study has been established to investigate the wellbore integrity at various conditions found underground. The results show that separation at the cement-casing interfaces is highly probable in injection wells. The abandoned wells will maintain their integrity within the first thousand years after exposure to CO_2-bearing fluids. Our observations suggest that the compaction of the cement-rock interfacial transition zone helps the cement sheath maintain its integrity for a longer period of time.

Keywords: CO_2 storage; Cement; Mechanics; Chemistry; Plastic-damage

1 Introduction

An increase in the level of greenhouse gases in the atmosphere is one of the main reasons for the increase in the global average temperature [1,2]. Carbon dioxide (CO_2) accounts for 9-26% of greenhouse gas emissions resulting from anthropogenic activities. Carbon capture and storage is one amelioration method to control the level of emitted CO_2. In CCS projects, captured CO_2 is injected into underground formations, depleted oil and gas reservoirs offering the greatest potential for underground storage of CO_2 [3]. There has been a broad study on the structure of these types of reservoirs. In addition, they have already proved to have been capable of accommodating high-pressure and high-temperature fluids for a long period of time hence making them ideal as the potential CO_2 storage sites [4,5].

The huge number of drilled oil and gas wells within these reservoirs around the world, however, puts the integrity of CCS projects at risk. The number of drilled wells in the USA, from 1859 to 1994, is reported to be around 3.2 million, of which 2.4 million were abandoned [6]. In the Texas state alone, more than one million abandoned wells exist [7], and it is estimated that this number is around 400,000 in the Alberta Basin in Canada [3]. The number of drilled wells in Australia and Brazil are 9,903 and 21,301, respectively [8]. If each could be a potential source of leakage, investigating wellbore integrity is a crucial prerequisite process prior to starting CO_2 injection for any CCS project.

Once the CO_2 is injected in underground formations, it begins moving laterally beneath the caprock generally towards less deeper locations [9–13]. Therefore the CO_2 plume would encounter other wells as it moves along its path. As a consequence, both the previously abandoned and present injection wells are possible leakage sources for the injected CO_2.

The dissolution of CO_2 in brine reduces the pH from some 13 to less than four depending on the conditions found underground [14]. An advection process is responsible for the renewal of CO_2-bearing fluids at the cement-brine interface [15–19]. CO_2-bearing fluids are transported into the inner parts of the cement matrix by the diffusion process [14,17–20]. This is due to the low permeability of the cement matrix, which is less than 200 μD [21], and the blockage of fluids at the cement-casing interface.

The invasion of CO_2 bearing fluids into the cement matrix degrades Portlandite (calcium hydroxide, CH), deep within the cement matrix [22,23]. The freed calcium cation diffuses outwards and precipitates at the locations close to the cement-brine interface. This phenomenon is referred to as the carbonation process and the corresponding area it occurs in is referred to as the calcite precipitation zone. The porosity decreases in this zone due to the precipitation of the calcite while the strength shows an increase [24]. Generally, cement carbonation can be considered as a linear diffusion phenomenon similar to $d = k\sqrt{t}$, where d is the depth of carbonation, t is time, and k is a constant which depends on the, relative humidity, water saturation, CO_2 concentration, cement type, and other surrounding conditions [25,26]. This is correct for civil engineering applications which are occurring at the conditions corresponded to the Earth's surface. Nevertheless, the harsh conditions found underground need a detailed investigation of the coupled effects of geochemical-geomechanical alterations. In this case, the concentration of CO_2 in brine is much higher than that at the Earth's surface and temperature is also higher. With the invasion of greater quantities of carbon species, calcium silicate hydrate at the outermost layers of the cement matrix is converted into an amorphous silica gel. The calcium carbonate (or calcite with the formula of $CaCO_3$) in the calcite precipitation zone also gradually re-dissolves in the CO_2-bearing fluids at a rate far less than the disintegration rate of C-S-H. The dissolution of Portlandite, the disintegration of C-S-H, and the re-dissolution of calcite is referred to as the degradation process. In contrast to the carbonation, the degradation process results in an increase in the porosity and a reduction in the strength of the affected zones [24,27–33].

The stress in the cement matrix results from the combination of the effect of the *in-situ* horizontal stress and the fluid pressure. In our calculations, the plane strain conditions are assumed to dominate the rock-cement-casing assemblage. The failure of the cement sheath,

especially at the cement-casing and the cement-rock interfaces, provides high leakage pathways for CO_2-bearing fluids to escape. In contrast to the softening effect of the failure process, the deformation phenomenon hardens the cement sheath, therefore increasing its durability. A high cohesive strength prevents the failure of interfacial transition zones i.e., the rock-cement and the cement-casing interfaces [34]. The cement matrix can withstand high compressive stresses while it is weak in regard to tensile stresses. The cementing job affects the stress distribution and the cracking index [35]. A non-uniform stress distribution accompanied by a reduction in the fluid pressure can result in the sand production and the deformation of the well casing [36,37]. Although an extensive study has been conducted on the geomechanical and geochemical evolution of the cement matrix, to the best of the authors' knowledge, there is no information available relevant to their coupled effect on the cement matrix resulting from the invasion of CO_2-bearing fluids.

In this paper, the performance of the rock-cement-casing assemblage is investigated using a chemo-mechanical model developed by the authors. In this chemo-mechanical model, the geomechanical part is coupled with the geochemical alterations which is improved using a plastic-damage model. This work provides a parametric study on the integrity of the wellbores in CO_2 storage sites. In Section 2, the model which has been used in this paper is introduced. A summary on the geochemical aspect is brought in Section 3. Then, the underlying method for updating parameters and boundary conditions are introduced in Section 4. In Section 5, the performance of the rock-cement-casing assemblage is investigated. In this section the effects of temperature, composition and porosity, *in-situ* horizontal stress, fluid pressure, the cement sheath thickness, pH, and the type of surrounding rocks are discussed, respectively. The prediction methodology will be explored in Section 5.8. Finally, all the results are concluded in Section 6.

2 Description of the model

The cement matrix is similar to a porous medium which is affected by the *in-situ* horizontal stress, the overburden stress, and the fluid pressure. The effective stress was introduced to account for the impact of the fluid pressure on the stress distribution [38–40]. The rock-cement-casing assemblage is assumed to be similar to a cylindrical coordinate system with a radial symmetry regarding casing axis (Please, refer to Figures 5 and 6 in [5]). Therefore, the distribution of the normal stresses can be obtained as follows [41–43]:

$$\sigma_r = \lambda'(\varepsilon_r + \varepsilon_\theta + \varepsilon_z) + 2\mu'\varepsilon_r + \alpha' p_f - (3\lambda' + 2\mu')\alpha_{CTE}\Delta T \quad (1)$$

$$\sigma_\theta = \lambda'(\varepsilon_r + \varepsilon_\theta + \varepsilon_z) + 2\mu'\varepsilon_\theta + \alpha' p_f - (3\lambda' + 2\mu')\alpha_{CTE}\Delta T \quad (2)$$

$$\sigma_z = \lambda'(\varepsilon_r + \varepsilon_\theta + \varepsilon_z) + 2\mu'\varepsilon_z + \alpha' p_f - (3\lambda' + 2\mu')\alpha_{CTE}\Delta T \quad (3)$$

where, σ_r, σ_θ, and σ_z are the stresses in the r-direction, the θ-direction, and the z-direction, respectively. ε_r, ε_θ, and ε_z are the strains in the r-direction, the θ-direction, and the z-direction, respectively. ΔT is the temperature change, α_{CTE} is the coefficient of thermal expansion, and p_f is the fluid pressure. λ', μ', and α' are Lame's constant, the shear modulus, and the Biot coefficient for a damaged rock, respectively, which can be defined as functions of the undamaged parameters as follows:

$$\alpha' = 1 - (1 - d_{tot})\frac{K}{K_s} \quad (4)$$

$$\lambda' = (1 - d_{tot})(K - \frac{2}{3}\mu) \quad (5)$$

$$\mu' = (1 - d_{tot})\frac{E}{2(1+\nu)} \quad (6)$$

where, d_{tot} is the total damage parameter (a scalar parameter) which shows the effective surface density of microdefects [43]. K and K_s are the bulk modulus of dry porous rocks and the bulk modulus of grains, respectively. E, μ, and ν are the Young's modulus, the shear modulus, and the Poisson's ratio, respectively. The plane strain assumption is also considered to dominate the rock-cement-casing assemblage.

2.1 Elastoplasticity

The cement matrix is an evolving quasi-brittle material based on an elastoplastic behaviour under cyclic loading. The cement matrix returns to its initial state after unloading within the elastic zone, while it keeps a residual change if the elastic-plastic boundaries are exceeded. This residual alteration, compared to the initial state after unloading, is referred to as the plastic-damage change. A model was introduced to characterise this behaviour by Lubliner et al. (1989). In the plastic-damage models, the core concept is based on the degradation of the cement stiffness due to the development of microcracks [45]. Therefore, the basic expression for the evolution of the stress can be written as follows:

$$\sigma = (1 - d_{tot})C : (\varepsilon - \varepsilon_p) \quad (7)$$

where, ε and ε_p are the total and the plastic strains. They are basically tensors, however, in Eq. (7), they are expressed as six-dimensional vectors to take advantage of the symmetry in their tensors. σ is the stress tensor, and C is the elasticity tensor. The total damage parameter in this paper is computed using the approach as suggested in [46].

The elastic-plastic boundaries form the failure envelope of a rock showing the zone where it will remain safe. The failure envelope basically is composed of two main sections including the failure and the cap surfaces. The failure refers to the process by which the rock loses its integrity while the deformation process increases the durability of the rock. The dilation process occurs after passing the failure surface, and the deformation process is a result of increasing the average compressive stress on the entire facets of the rock [47–49].

The failure processes includes the tensile and the shear failures. The tensile failure is a function of the minimum stress, σ_{min}, and is characterised by η_t as the tensile failure criterion [50,51]. The tendency of the rock towards shear failure also increases with increasing the difference between the maximum stress, σ_{max}, and the minimum stress, σ_{min} [52]. The shear failure surface area is described using the Drucker-Prager criterion [53]. The rock will fail once the shear failure criterion, η_s, becomes larger than one. The cap surface characterises the area where the rock is compacted due to a significant average compressive stress exerted upon the rock. An elliptical function was applied to show the elastic-compaction boundary [54–58]. The hardening process occurs once the deformation criterion, η_d, increases to greater than one. For more details on the failure and deformation criteria, please refer to

Appendix A. The uniaxial compressive strength of the cement matrix is calculated as follows [59]:

$$f_{c,cement} = k_s(1-\gamma)(\frac{10^6 E_{cement}}{43\rho^{1.5}}) \quad (8)$$

where, ρ is density in kg/m^3, and $f_{c,cement}$ is the uniaxial compressive strength for the cement matrix in MPa, and k_s is a coefficient which depends on the cement type, the value of 2.31 being chosen representing k_s for CEM I 42.5R, γ shows the volume ratio of aggregates, this value is assumed to be zero based on using the plain cement paste for well-cementing job. The uniaxial tensile strength (UTS) of the cement matrix is calculated as follows [60]:

$$f_{t,cement} = 1.04 f_{tsp,cement}^{0.87} \quad (9)$$

where, $f_{tsp,cement}$ is the splitting tensile strength of the cement matrix defined as [61]:

$$f_{tsp,cement} = 0.387 f_{c,cement}^{0.63} \quad (10)$$

The failed and deformed (altered) zones undergo mechanical alterations which affect their strength and fluid flow properties (porosity and permeability). From the mechanical point of view, an altered rock is considered to be composed of the intact and the altered parts, as shown in Figure 1. The altered parts are similar to the planar surfaces developing across the rock based on the stress state and the type of the mechanical alteration (the tensile failure, the shear failure, and the deformation). These altered parts in the rocks have been extensively studied and are referred to as bands, and classified as follows [47–49,62–67]:

- Pure dilation bands
- Dilation shear bands
- Compaction shear bands

The pure dilation bands express the formation of cracks due to the tensile failure in the rock [47]. The porosity within these cracked areas is assumed to increase to 100%. The bands formed due to the shear dilation show an increase of 8% in porosity while the porosity in the compaction shear bands decreases by one order of magnitude [49].

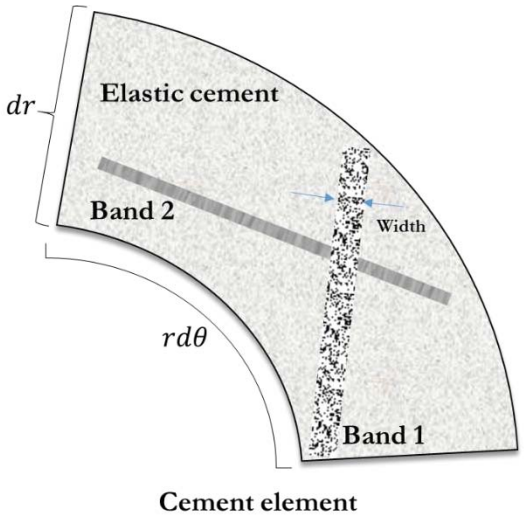

Figure 1. A cement element composed of the embedded bands and the elastic parts.

Bands are introduced in this paper as a methodology to properly involve the contribution of altered zones in the evolution of the fluid flow properties. As can be seen in Figure 1, an altered cement element composed of the elastic parts and the bands. Therefore, the porosity of the element, $\phi_{element}$, can be written as:

$$\phi_{element} = s_{band\,1}\phi_{band\,1} + s_{band\,2}\phi_{band\,2} + s_{elastic\,cement}\phi_{elastic\,cement} \quad (11)$$

where,

$$s_{band\,1} + s_{band\,2} + s_{elastic\,cement} = 1 \;\&\; s_i = V_i/V_{tot} \quad (12)$$

where, V_i and V_{tot} are the volume of the part i (band 1, band 2, or the elastic part), and the total volume, respectively. s_i is the volume fraction of the part i. $\phi_{band\,1}$, $\phi_{band\,2}$, and $\phi_{elastic\,cement}$ show the porosity of band 1, band 2, or the elastic part, respectively.

3 Geochemistry

The invasion of CO_2-bearing fluids into the cement matrix could result in either the carbonation or the degradation processes within it [14,68]. It can be deduced that the former expands the failure envelope of the cement matrix due an increase in the UCS and the latter leads to the shrinkage of the failure envelope of the cement matrix due to a reduction in the UCS (please, refer to [69] see the effect of carbonation and degradation processes on the UCS). The surrounding rocks of the cement sheath are also affected by CO_2-bearing fluids. The intensity of the alteration within the rocks depends on their mineral composition. The pH level of the CO_2-bearing fluids in the sandstone formations remains approximately constant. The dissolution of calcium carbonate increases the pH of CO_2-bearing fluids in limestone formations [70]. In this paper, although the chemical composition of CO_2-bearing fluids is affected by the surrounding formations, the rocks themselves are assumed not to be significantly altered due to chemical reactions. In fact, the rocks are considered to be in an equilibrium state with the CO_2-bearing fluids. Therefore, from a geochemical perspective, the cement sheaths adjacent to the sandstone formations will be more vulnerable to the degradation process compared to the cement sheaths adjacent to the limestone formations. The chemical calculations are run using the CrunchFlow code developed by Steefel et al. (2015) based on the following equation:

$$\frac{\partial\left(\phi S_\beta C_{j_\beta}\right)}{\partial t} = \nabla.\left(\emptyset S_\beta D^*_{j_\beta} \nabla C_{j_\beta}\right) - \nabla.\left(q_\beta C_{j_\beta}\right) + R_{j_\beta} + \zeta_{j\beta} + S_{j_\beta}, \quad (j = 1,2,3,\ldots n) \quad (13)$$

where, S_β is the saturation of the phase β, C_{j_β} is the concentration of the component j in the phase β, $D^*_{j_\beta}$ is the diffusion coefficient of the component j in the phase β, q_β is the velocity vector of the phase β, R_{j_β} is the net rate of the produced component j in the phase β due to the chemical reactions, $\zeta_{j\beta}$ is the interphase mass transfer of the component j out/into the phase β, and S_{j_β} shows the mass transfer of the component j between an external source and the phase β. R_{j_β} and $\zeta_{j\beta}$ are scalar numbers.

4 Numerical approach

In this paper, it is assumed that CO_2 is completely dissolved in brine, and the pores of the surrounding formations and the cement sheath are filled with a single phase fluid. The temperature and pressure in CO_2 storage sites is higher than the critical temperature (31.1 °C) and pressure (7.38 MPa) of CO_2, respectively. This means that CO_2 will be in a supercritical state. Although calculations in this paper consider the maximum dissolution of CO_2 in brine, the concentration of CO_2 in brine is generally less than this value. This is due to the CO_2 escaping from CO_2-bearing fluids, and other CO_2 trapping mechanisms occurring prior to the CO_2 plume encountering the cement-brine interface.

As shown in Figure 2, an iterative approach is applied to couple the geochemical and geomechanical calculations. The geochemical calculations are pressure independent due to the full dissolution of CO_2 in brine and the single phase fluid dominance over the pores of the cement and the rock. At the time step, t, the porosity and the mineral composition of the cement matrix is updated using the geochemical simulation and then imported into the section of the geomechanical simulation. The porosity profile as the main controlling property is updated applying the geomechanical simulation. The porosity profile is imported into the geochemical simulation for the next time step, $t + 1$. The new porosity profile, ϕ_{new}, can be defined as:

$$\phi_{new} = \phi_c + \Delta\phi_m + \Delta\phi_b \quad (14)$$

where, ϕ_c is the porosity after imposing geochemical calculations, $\Delta\phi_m$ and $\Delta\phi_b$ are the porosity change due to the imposed stress state and the formation of bands, respectively. The flowchart in Figure 2 cycles to the point where the entire cement sheath disintegrates due to either the shear or the tensile failures.

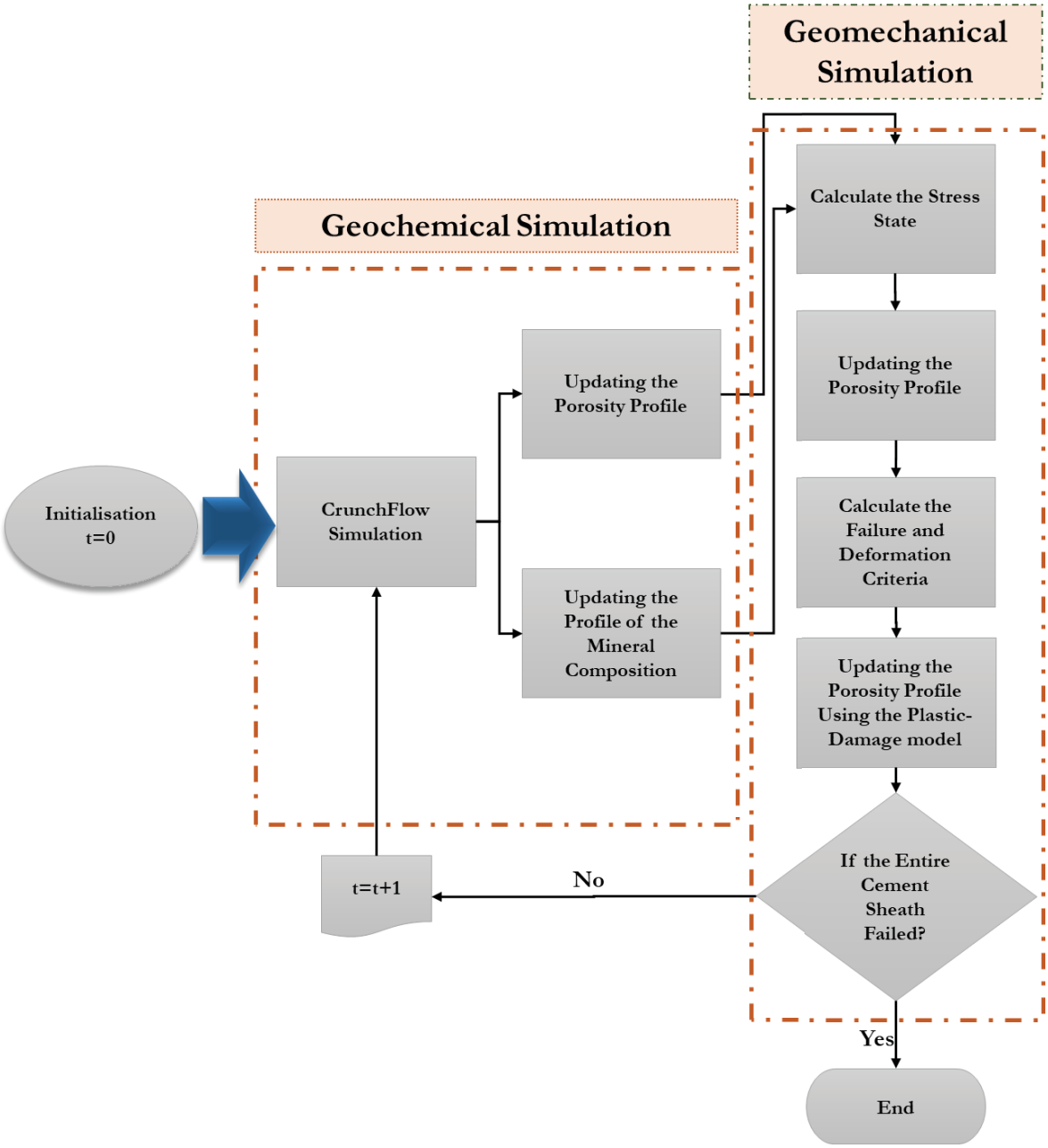

Figure 2. The flowchart for coupling the geomechanical and geochemical alterations

At the initial state, ($t = 0$), the boundary conditions for the stress distribution are as follows:

$$\sigma_r = \sigma_{in-situ} \; on \; r = R_{th} \quad (15)$$

$$\sigma_r = p_{inside} \; on \; r = R_{i,casing} \quad (16)$$

where, $\sigma_{in-situ}$ is the *in-situ* horizontal stress, R_{th} is the thermally influenced radius of the rock-cement-casing assemblage which is considered to be 1079.5 mm [72,73], p_{inside} is the inside pressure, $R_{i,casing}$ is the inner radius of the casing.

It is assumed that the cement sheath is exposed to an infinite source of CO_2-bearing fluids. Therefore, the Dirichlet boundary condition dominates at the cement-rock interface. The fluid flow at the cement-casing interface is zero due to the blockage of flow at this interface. Consequently, the no-flow boundary conditions dominate the cement-casing interface. These

boundary conditions corresponding to the geochemical characterisation remain constant with time. The no-flow boundary conditions at the casing-cement interface signify the dominance of the diffusion process over the geochemical alteration within the cement matrix. On the other hand, the steady concentration of the carbon species in the areas within the formation close to the cement-brine interface shows that the advection process is responsible for the renewal of the carbon species. It is worth noting that the low permeability of the cement matrix (generally less than $200\ \mu D$, [21]) and the blockage of flow at the cement-casing interface trivialises the role of the advection process within the cement sheath. The initial stress and geochemical boundary conditions are subject to change with time. The failure of ITZs and the entire cement sheath alters the governing boundary conditions initially assumed to dominate the rock-cement-casing assemblage.

The basic cement, rock, and casing properties are similar to those defined in [74] except those parameters which have been changed in each section to be studied. For more details on the properties, please refer to Appendix B and Figures 5 and 6 in [5] to see the configuration. The model developed by Bagheri et al. [74] simulates the alteration in the rock-cement-casing assemblage for the wellbores in CO_2 storage sites. In this model, it is assumed that the cementing job was flawlessly conducted. In these simulations, the rock-cement-casing assemblage has a cylindrical form, along with the interface boundaries. The wellbores are considered to be impacted by the normal *in-situ* horizontal stress, and the plane strain conditions govern the stress distribution. It is assumed that the wellbores pass a normal loading path without being affected by abnormal creeping or tectonic displacements. The composition of the cement matrix is similar to class H surrounded by a sandstone rock unless in Section 5.7 in which the effect of limestone is investigated. In this paper, the most outstanding results are represented in the figures, and the other outcomes are referred to and interpreted in each section.

5 Results and discussion

In this paper, we have attempted to evaluate the performance of the rock-cement-casing assemblage using the methodology developed in [74]. In fact, this work provides a general framework illustrating the ultimate lifespan of the cement sheath under different conditions found in CO_2 storage sites. A parametric study was conducted in which the integrity of the rock-cement-casing assemblage was studied. This study includes the effect of temperature, composition and porosity, *in-situ* horizontal stress, fluid pressure, the cement sheath thickness, pH, and the type of surrounding formations.

5.1 Temperature

The temperature of the underground formations, T_e, is a function of the depth. The average gradient of temperature is considered to be equal to 30 ℃$/km$ [75], and the temperature at the Earth's surface is assumed to be 20 ℃. Therefore, T_e can be calculated as follows:

$$T_e = 20 + 0.03d \qquad (17)$$

where, d is depth in metres and T_e is the underground formation temperature in centigrade. The temperature reduction, ΔT, in the casing is assumed to be constant while it is considered to reduce in a logarithmic manner within the cement-rock part as follows [72,73,76]:

$$\Delta T = \begin{cases} T_w - T_e & r \le R_{o,casing} \\ T_w - T_e + \dfrac{(T_e - T_w)\log\left(\dfrac{r}{R_{o,casing}}\right)}{\log\left(\dfrac{R_{th}}{R_{o,casing}}\right)} & R_{o,casing} < r \le R_{th} \end{cases} \quad (18)$$

where, T_w is the well temperature, r is the radius, and $R_{o,casing}$ shows the outer radius of the casing. In this paper, the inner radius of the well casing, $R_{i,casing}$, is 6.366 inches and the outer radius of the well casing, $R_{o,casing}$, is 7 inches. The effect of the temperature reduction is significant in the injection wells. In abandoned wells, the temperature reaches an equilibrium with the surrounding formations. Therefore, the temperature reduction in them is equal to zero. The fluid pressure at each depth is assumed to be equal to the hydrostatic pressure.

In this case, the well temperature, T_w, increases from 30 ℃ to the temperature of the underground formations, T_e. It should be noted that the minimum temperature inside the well is considered to be equal to 30 ℃ as a representative value adopted from [77,78]. The temperature reduction in the well, ΔT_w, is equal to $(T_w - T_e)$. The maximum temperature difference between the underground formations and the well can be calculated as follows:

$$\Delta T_{max} = 10 - 0.03d \quad (19)$$

The cement-casing interfacial transition zone is highly probable to fail due to the tensile stress. As can be observed in Figure 3 (a), at low well temperatures and deep within the matrix, the cc fails a short time after the CO_2 injection commences. Figure 3 (b) and (c) show that the cement-rock interfacial transition zone will fail at the middle well temperatures. It can be observed that the cc and the cr maintain their integrity for a long period of time at other well temperatures. The minimum expected lifespan of the cement sheath is 1897 years, as shown in Figure 3 (d). The lifespan of the cement sheath with depth increases by more than two orders of magnitude. The shear dilation and the deformation processes are not expected to affect the cc. The cr is compacted prior to the 30th day of the CO_2 injection. For the cement sheath, it is predicted that the pure dilation and compaction processes will not occur in less than 10^5 years. It can be seen that the cc and the cr fail at the specific depths and temperatures, as shown in Figure 3, in contrast to the cement sheath, which at least maintains its integrity for more than one thousand years. This denotes that the cement sheath is inclined to be separated from the casing and the rock surface, although the cement sheath will retain its integrity. This is due to the short period of the CO_2 injection processes, which probably in many projects would be less than a century.

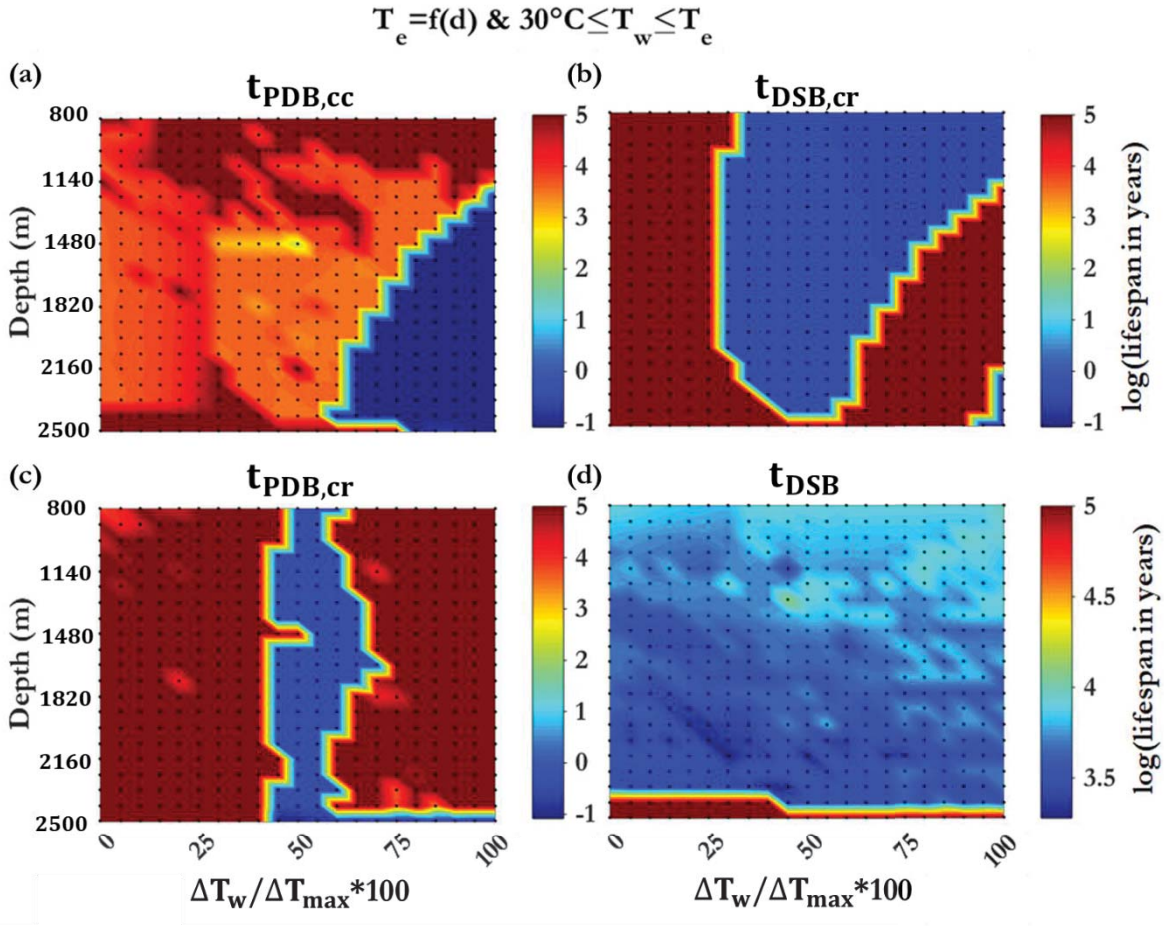

Figure 3. (a) The tensile failure time of the cement-casing interfacial transition zone; (b) the shear failure time of the cement-rock interfacial transition zone; (c) the tensile failure time of the cement-rock interfacial transition zone; (d) the Shear failure time of the cement sheath at a constant formation temperature, T_e, and different well temperatures, T_w. Colour bars on the right side of figures show the logarithm of the lifespan for that section with base 10, for example, 2 means that section will deform or fail after 10^2years depending on the active process. Title of each figure demonstrates the time for the formation of a specific band within a section, for example, $t_{PDB,cc}$ shows the time for the formation of PDB at the cc location, or t_{PDB} shows the time for the formation of PDB within the cement matrix.

Figure 4 shows the case where the temperature of the well is 30 ℃ and the temperature of the formation increases from T_w to the maximum value calculated by Eq. (17). In this case, it can be seen in Figure 4 (b) and (c) that the cr loses its integrity at the middle range of the formation temperatures. The cr is compacted (or deformed) during the first days of CO_2 injection. The cc falls apart at the high formation temperatures and the deep locations, as can be observed in Figure 4 (c). The shear dilation and the deformation processes do not influence the cc. Figure 4 (d) shows that the cement sheath retains its integrity for a minimum of 1938 years. The pure dilation and the deformation are not expected to affect the cement sheath in less than 10^5 years.

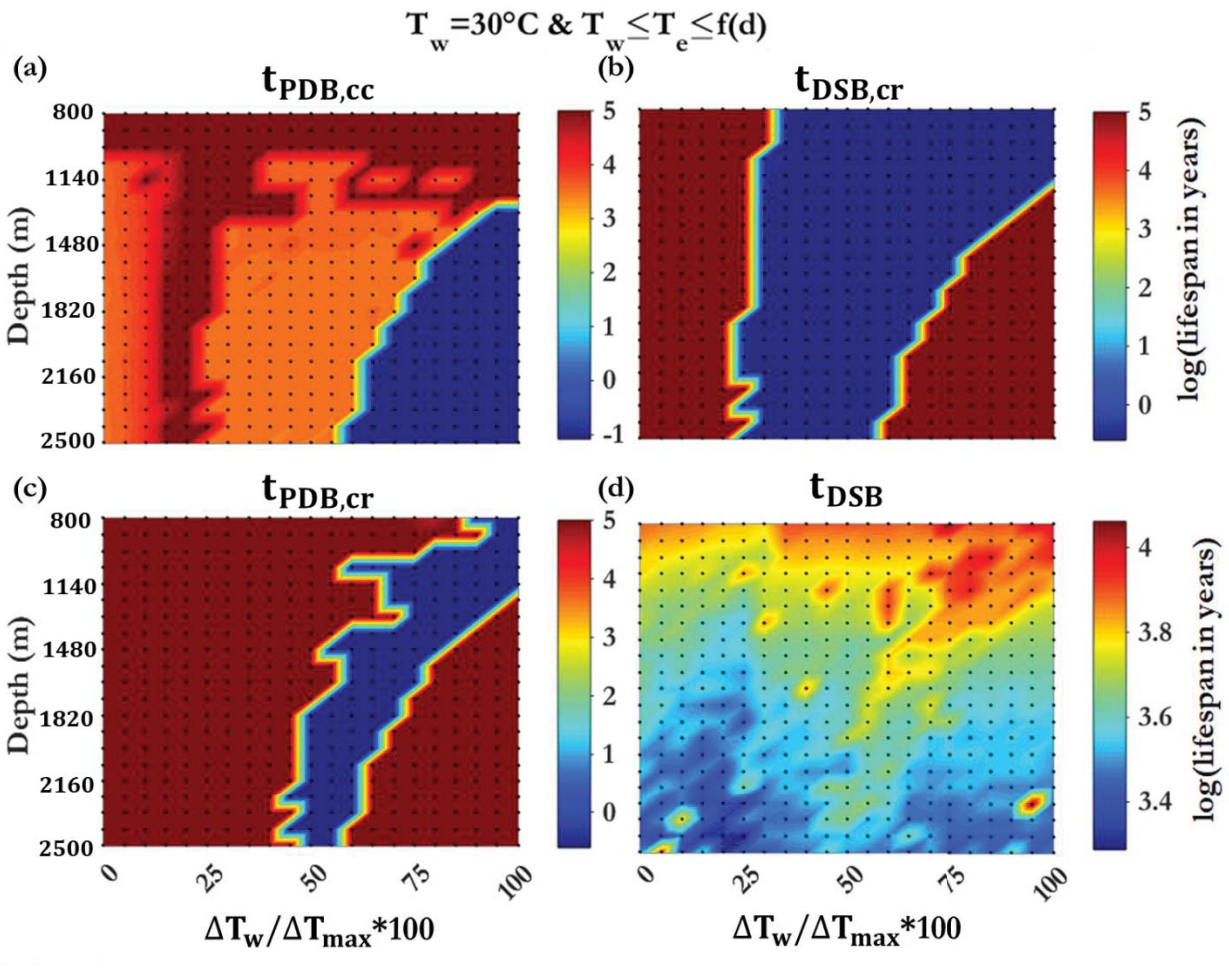

Figure 4. The tensile failure time of the cement-casing interfacial transition zone; (b) the shear failure time of the cement-rock interfacial transition zone; (c) the tensile failure time of the cement-rock interfacial transition zone; (d) the Shear failure time of the cement sheath at a constant well temperature, T_w of 30 °C while the formation temperatures, T_e, changes from T_w to a maximum presented by Eq. (17).

The performance of the cement sheath and the ITZs are outlined in Table 1. It is concluded that the cement sheath maintains its integrity for an indefinite time interval. The cc is debonded due to the formation of PDB at deep locations where there is a high temperature difference between the formation and the well. The cement sheath is separated from the rock due to the formation of DSB and PDB at the middle range of temperature differences between the formation and the well. Subsequently, the cr will fully be compacted.

Table 1. The alteration of the cement sheath and the ITZs as a function of the temperature profile in the injection wells.

Zone	**The altering process**		
	DSB	**PDB**	**CSB**
Cement-casing interface	The cc is not affected.	In deep wells and at high temperature differences between the formation and the well, the separation of the	The cc is not affected.

		cement sheath from the casing occurs.	
Cement-rock interface	At the middle range of temperature differences between the formation and the well, the formation of DSB is expected.	At the middle range of temperature differences between the formation and the well, the formation of PDB is expected.	The cc is fully compacted during the first days after starting CO_2 injection process.
Cement sheath	The minimum time calculated is more than 1897 years.	The cement sheath is not affected.	The cement sheath is not affected.

5.2 Composition and porosity

Portlandite and calcium silicate hydrates are the main component minerals of the cement matrix. In this section, the effect of these two minerals on the durability of the rock-cement-casing assemblage is examined. The composition and the porosity of the cement matrix vary according the intervals given in Table 2.

Table 2. The range considered for investigating the effect of the mineral composition and the porosity.

Mineral phase composition (Vol. %) in the solid part	Portlandite ($\boldsymbol{x_{CH}}$)	15-35%
	C-S-H (x_{C-S-H})	85-65%
Porosity ($\boldsymbol{\phi}$)	5-25%	

5.2.1 Injection wells

The lifespan of the cement sheath and ITZs are shown as a function of the porosity and the mineral composition of Portlandite in Figures 5 and 6. At the depth of 800 m, the cr fails due to the tensile stress at high porosities, as presented in Figure 5. Table 3 summarises that for an injection well the tendency of the cr to fail due to the tensile stress decreases with increasing in depth. Figure 6 (a) illustrates that the cr dilates due to the shear stress throughout most ranges of porosity and Portlandite composition except at a porosity of 5% and x_{CH} greater than or equal to 25%. Table 3 indicates that the cc is subject to tensile failure at depths of 1650 and 2500 m while it remains safe at the depth of 800 m. The cr collapses due to both tensile and shear stresses, except at high Portlandite compositions and low porosities at the depth of 800 m as shown in Figure 5. The cr is compacted at depths from 800-2500 m. Furthermore, the minimum lifespan of the cement sheath is 663 years, which is far higher than the lifespan of a normal CO_2 injection project.

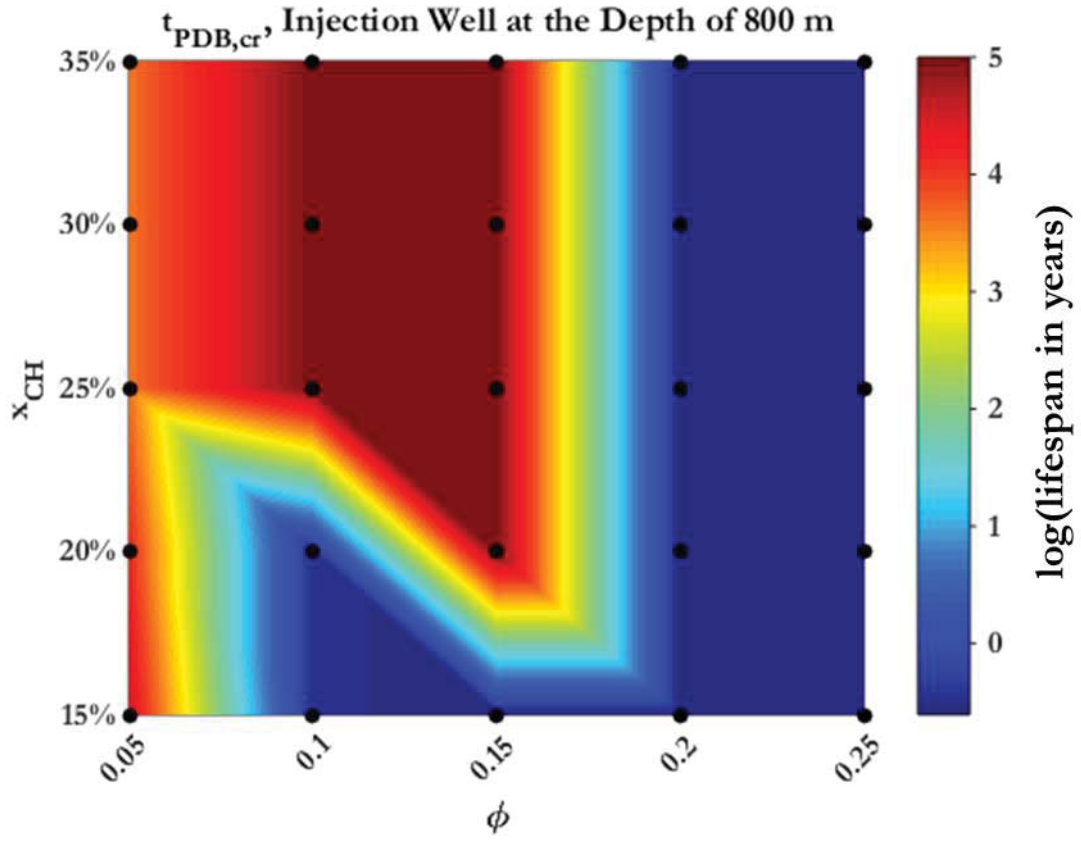

Figure 5. The tensile failure time of the cement-rock interfacial transition zone at the depth of 800 m as a function of the porosity and Portlandite composition.

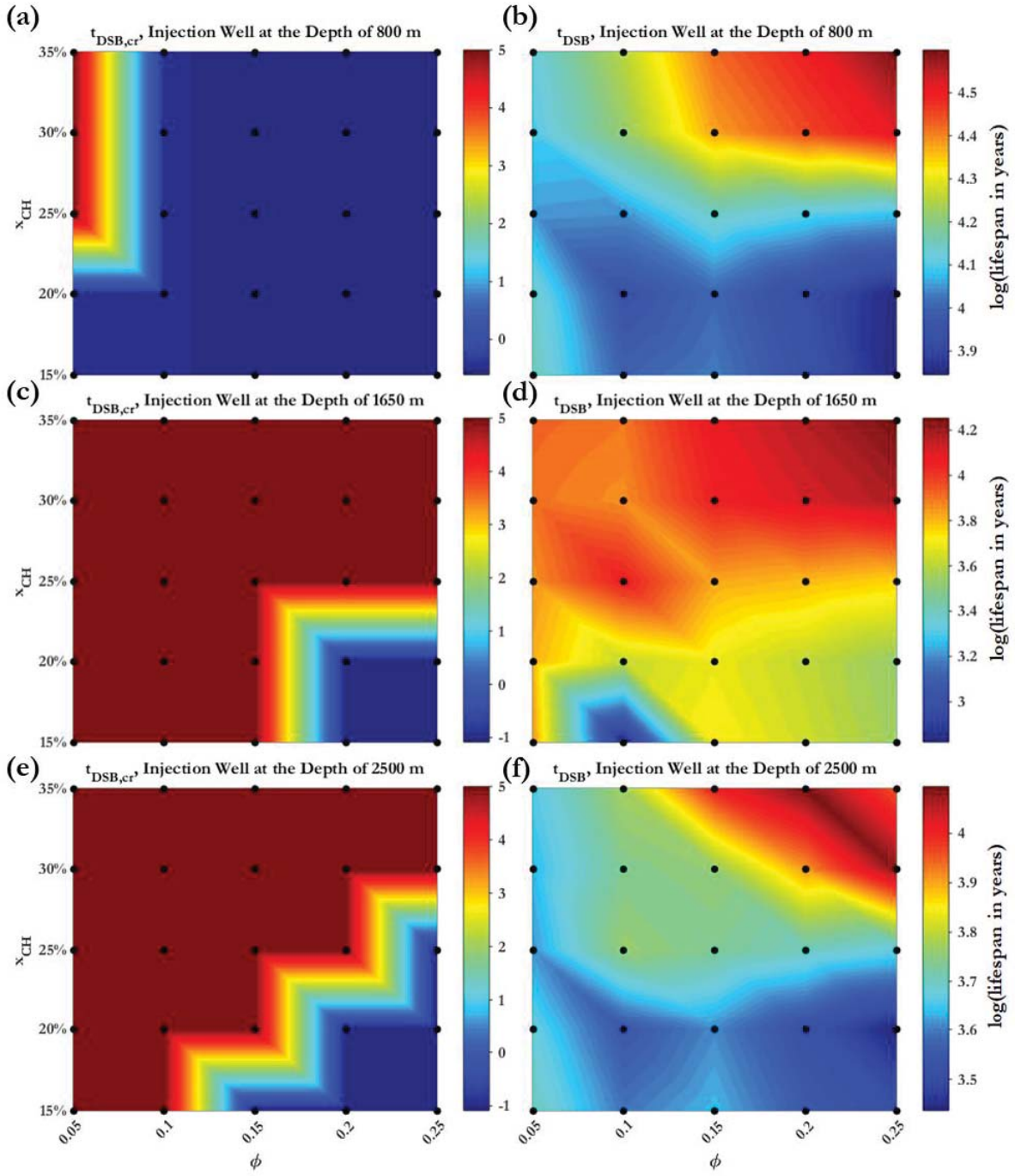

Figure 6. The shear failure time of (a) the cement-rock interfacial transition zone at the depth of 800 m; (b) the cement sheath at the depth of 800 m; (c) the cement-rock interfacial transition zone at the depth of 1650 m; (d) the cement sheath at the depth of 1650 m; (e) the cement-rock interfacial transition zone at the depth of 2500 m; (f) the cement sheath at the depth of 2500 m.

Table 3. The alteration of the cement sheath and the ITZs as a function of the composition and porosity of cement sheaths in injection wells.

Depth (m)	Zone	The minimum lifespan (years)		
		DSB	PDB	CSB

800	**Cement-casing interface**	3143	7995	10^5
	Cement-rock interface	0.2466	0.2466	Early compaction at all porosities and Portlandite compositions.
	Cement sheath	6999	10^5	10^5
1650	**Cement-casing interface**	661	Early dilation at all porosities and Portlandite compositions.	10^5
	Cement-rock interface	0.0822	494	Early compaction at all porosities and Portlandite compositions.
	Cement sheath	663	1198	10^5
2500	**Cement-casing interface**	1220	Early dilation at all porosities and Portlandite compositions.	638
	Cement-rock interface	0.0822	10^5	Early compaction at all porosities and Portlandite compositions.
	Cement sheath	2353	10^5	3043

5.2.2 Abandoned wells

The effect of the mineral composition and porosity are also investigated in abandoned wells. Figure 7 shows the predicted lifespan of the cement sheath at several depths for various values of porosity and mineral composition. The cement sheath preserves its integrity for more than a thousand years. Table 4 lists the minimum lifespan of the cement sheath and the ITZs. The cr is compacted during the first days of being exposed to CO_2-bearing fluids.

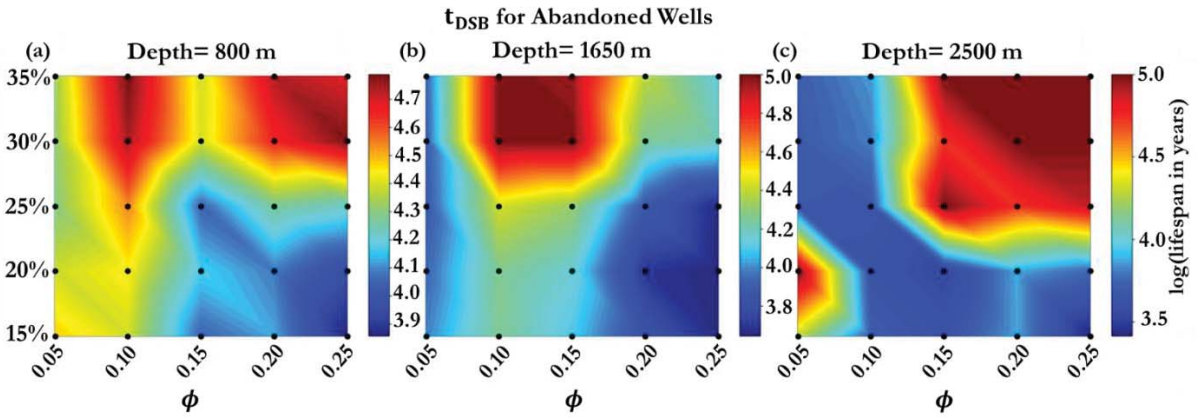

Figure 7. The shear failure time of the cement sheath for an abandoned well (a) at 800 m; (b) 1650 m; (c) and 2500 m.

Table 4. The alteration of the cement sheath and the ITZs as a function of the composition and porosity in abandoned wells.

Depth (m)	**Zone**	**The minimum lifespan (years)**		
		DSB	**PDB**	**CSB**
800	**Cement-casing interface**	4514	3736	10^5
	Cement-rock interface	10^5	1775	Early compaction at all porosities and Portlandite compositions.
	Cement sheath	7199	10^5	10^5
1650	**Cement-casing interface**	3174	1701	10^5
	Cement-rock interface	10^5	2545	Early compaction at all porosities and Portlandite compositions.
	Cement sheath	4419	10^5	10^5
2500	**Cement-casing interface**	2721	1628	1664
	Cement-rock interface	10^5	6000	Early compaction at all porosities and Portlandite compositions.
	Cement sheath	2596	2178	4725

5.3 In-situ horizontal stress

The *in-situ* horizontal stress, $\sigma_{in-situ}$, is the main acting stress on the rock-cement-casing assemblage. Based on the plane strain assumption, the *in-situ* horizontal stress motivates the stresses in the z-direction and the θ-direction. The value of the *in-situ* horizontal stress is a function of the lithostatic stress depending on the formation type and circumstances. This section attempts to evaluate the impact of the *in-situ* horizontal stress on the wellbore integrity. The *in-situ* horizontal stress is assumed to act on the thermally influenced radius, R_{th}, of the rock-cement-casing assemblage. The fluid pressure, p_f, is equal to the hydrostatic pressure, p_h. In this paper, the minimum $\sigma_{in-situ}$ is assumed to be equal to $p_f/0.7$ to prevent the formation of hydraulic fractures. Indeed, the horizontal stress could not be less than $p_f/0.7$ otherwise the fluid pressure would be able to create the hydraulic fractures which are perpendicular to the horizontal axis. The threshold $0.7\sigma_{in-situ}$is considered as the maximum value for the fluid pressure which is plausible to be operated in an injection process. The maximum bound of $\sigma_{in-situ}$ is assumed to be equal to $(40.5 + 0.014d)$ in MPa where d is the depth in meter [79]. Therefore, $(\Delta\sigma_{in-situ})_{max}$ can be defined as follows:

$$(\Delta\sigma_{in-situ})_{max} = (40.5 + 0.014d) - \frac{p_f}{0.7} \quad (20)$$

$(\Delta\sigma_{in-situ})_{max}$ shows the ultimate value which can be assumed to be added to $\sigma_{in-situ}$ if its minimum value supposed to be equal to $p_f/0.7$. Therefore, the increase in $\sigma_{in-situ}$ from its minimum value can be expressed as follows:

$$\Delta\sigma_{in-situ} = \sigma_{in-situ} - \frac{p_f}{0.7} \quad (21)$$

5.3.1 Injection wells

In the injection wells, the integrity of the cement sheath is not impacted by increasing the in-situ horizontal stress. The cr is compacted at all depths and values of $\sigma_{in-situ}$. As shown in Figure 8, the tensile and shear failures reduce the lifespan of the cc and the cr, respectively. Figure 8 (a) shows that the cc maintains its integrity at a depth of 800 m for the entire range of the in-situ horizontal stress while it fails at deeper wells. At the depth of 800 m, the cr disintegrates, as shown in Figure 8 (b). For an injection well at any depths and *in-situ* horizontal stress, it can be comprehended that the debonding of either the cc or the cr is inevitable. The formation of DSB occurs prior to the formation of the CSB at the cr location. It should be noted that in these calculations DSB and CSB are not possible to be simultaneously formed. This is due the distinct areas of activity for DSB and CSB in the failure envelope.

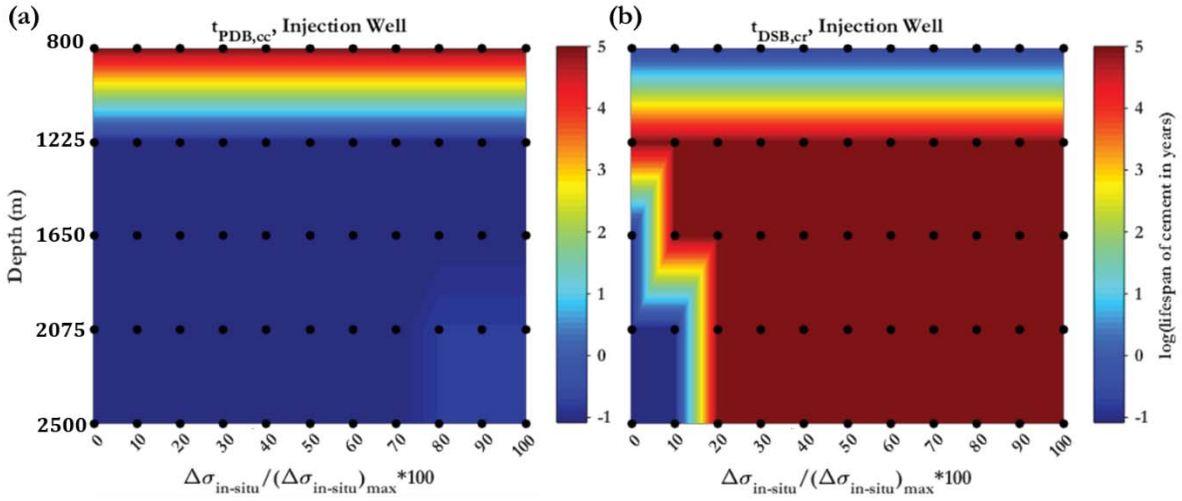

Figure 8. The failure time of (a) the cement-casing interfacial transition zone due to the tensile stress; (b) and the cement-rock interfacial transition zone due to the shear stress for an injection well.

5.3.2 Abandoned wells

In abandoned wells, it is predicted that the failure of the cement sheath and ITZs will not occur in less than 1666 years. The deformation process compacts the cr during the first 50 days after exposure to CO_2-bearing fluids. The cc and the cement sheath are also subject to the deformation process within the time scale displayed in Figure 9. The deformation time of the cc and the cement sheath decreases with increasing in depth and *in-situ* horizontal stress.

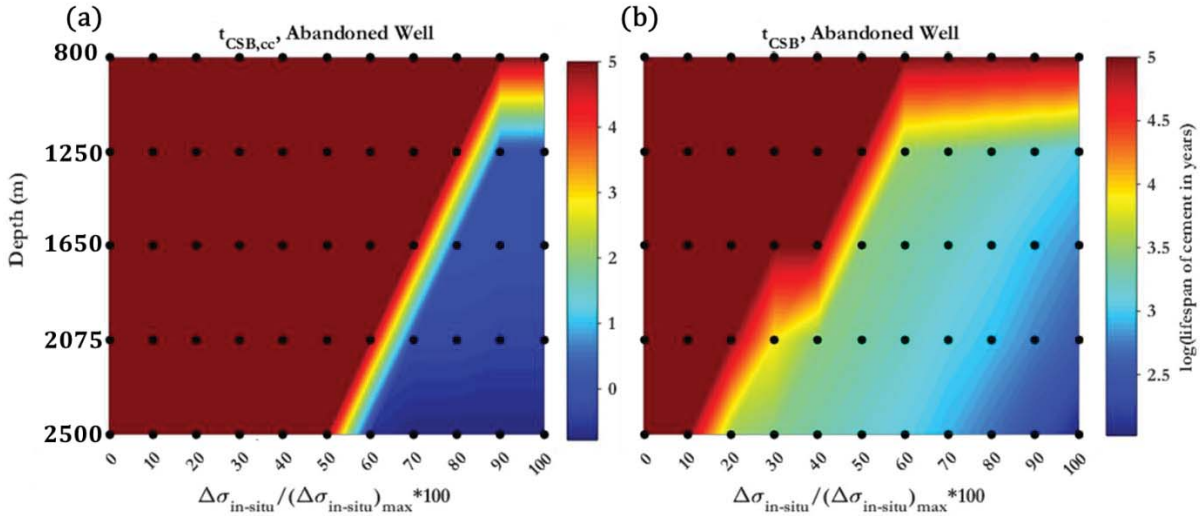

Figure 9. The compaction time of (a) the cement-casing interfacial transition zone; (b) and the cement sheath for an abandoned well.

5.4 Fluid pressure

The fluid pressure, p_f, is basically assumed to be equal to the hydrostatic pressure. Increasing the fluid pressure leads to an increase in the CO_2 concentration, however, it does not exceed the maximum concentration calculated by thermodynamic rules. In addition, rocks generally

show a reduction in the strength with increasing moisture content. The effect of the fluid pressure on the wellbore integrity is examined in this section for injection wells. The injection pressure changes from the hydrostatic pressure to $0.7\sigma_{in-situ}$. The maximum of p_f is chosen as the upper safety boundary to prevent the formation of hydraulic fractures. Therefore, the maximum increase in the fluid pressure can be defined as:

$$(\Delta p_f)_{max} = 0.7\sigma_{in-situ} - p_h \quad (22)$$

The value of the fluid pressure could become greater than $0.7\sigma_{in-situ}$, but the tendency of the hydraulic fracturing also increases. In this paper, $0.7\sigma_{in-situ}$ is considered as a safe threshold preventing the formation of hydraulic fractures.

$$\Delta p_f = p_f - p_h \quad (23)$$

where, p_h is the hydrostatic pressure, and Δp_f indicates the increase in the fluid pressure. The fluid pressure is highly likely to vary close to the injection wells due to the injection pressure at the bottom of the wellbore. In contrast, the fluid pressure in abandoned wells reaches an equilibrium sometime after being left. Therefore, in this section, the alteration of the fluid pressure is only considered in the injection wells.

The cr is compacted over the entire range of the fluid pressures and depths in an injection well, however, the DSB and PDB will result in failure of this zone, as shown in

Figure 10. At the depth of 800 m, the cr encounters tensile failure during the first 30 days after the start of the CO_2 injection process (except at $p_f = p_h$), as shown in Figure 10 (c). At depths deeper than or equal to 1225 m, the PDB is not expected to be created at the cr location. Besides, the cc will not be affected by the deformation process or the shear stress. The cement sheath retains its integrity for a long period of time. Therefore, it can be realised that under any stress state, either the cr or the cc fails while the cr is compacted over the entire range of the fluid pressures and depths in an injection well. Nevertheless, the cement sheath remains intact for a minimum of 3175 years.

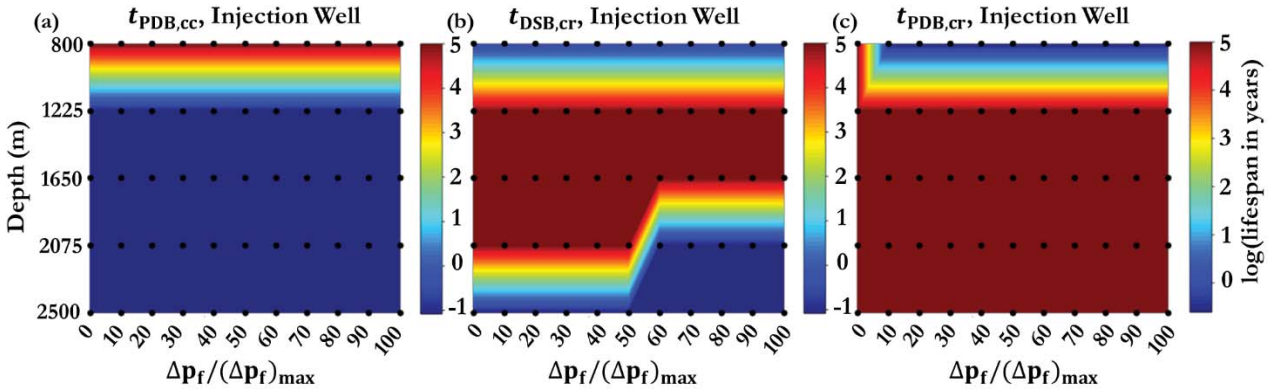

Figure 10. The failure time of (a) the cement-casing interfacial transition zone due to the tensile stress; (b) the cement-rock interfacial transition zone due to the shear stress; and (c) the tensile stress.

5.5 The cement sheath thickness

The normal thickness of the cement matrix in the calculations in this paper, is equal to 1.18 inches. Nevertheless, the weak parts of the formation wall, which are close to the cement, are highly probable to be dislodged during the cementing job. In addition, the effects of drill bits on the formation wall can also change the outer radius of the cement sheath. In this section, the impact of the cement sheath thickness on the stability of the rock-cement-casing assemblage is studied. The inner diameter of the cement sheath is 7 inches, and the ratio of the cement sheath thickness over the inner radius of the casing, $R_{i,casing}$, is assumed to change from 0.07 to 2.74. The inner diameter of the casing is 6.366 inches.

5.5.1 Injection wells

In this case, the cr is compacted over the entire range of the cement sheath thicknesses and all depths. The PDB is not expected to be formed at the cr location in the near future. Figure 11 (b) shows that the performance of DSB is limited to a depth of 800 m and t/r less than 2.74. The cr is not affected by the DSB with increasing depth and t/r (the ratio of the cement sheath thickness over the inner radius of the casing). As shown in Figure 11 (a), the cc is only influenced at the locations deeper than 800 m, and other alteration processes have no impact on its durability. Figure 11 indicates that in a CO_2 injection well, at least one of the cc or the cr will fail. In fact, increasing in the thickness of the cement sheath cannot stop the failure processes at either the cc or the cr places except at t/r of 2.74 at the depth of 800. In addition, none of the failure and deformation processes are predicted to impact the cement sheath in time periods of less than one thousand years.

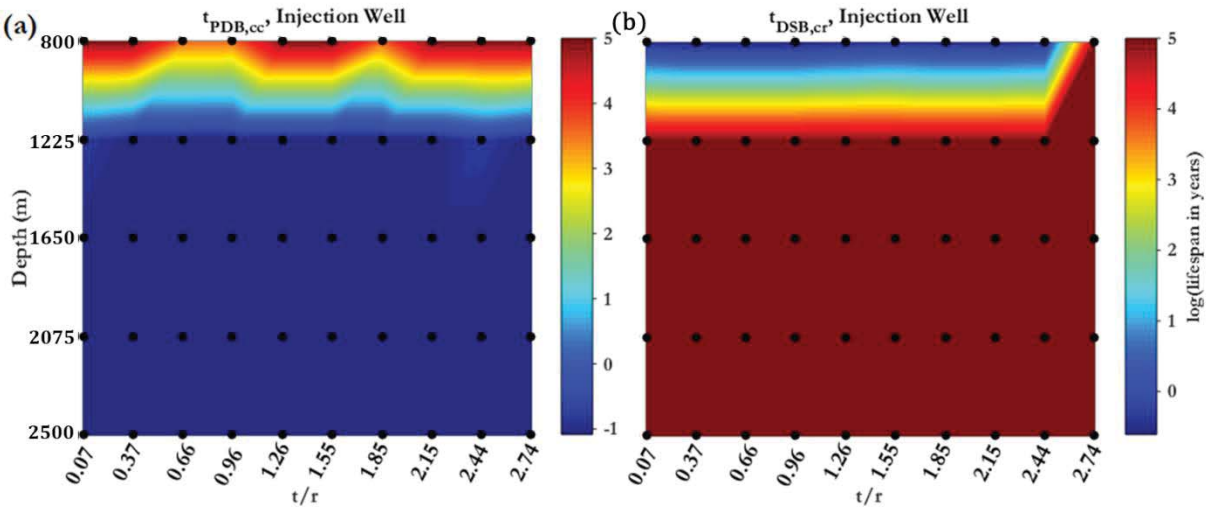

Figure 11. The failure time of (a) the cement-casing interfacial transition zone due to the tensile stress; and (b) the cement-rock interfacial transition zone due to the shear stress at the different thicknesses of the cement sheath.

5.5.2 Abandoned wells

In abandoned wells, the only active alteration phenomenon is the CSB process compacting the cr. The cr is compacted within the first days after being exposed to CO_2-bearing fluids. This process helps the cement sheath in maintaining its integrity for a longer period of time. The cc and cement sheath show no alteration in time frames of less than one thousand years.

5.6 pH

The reactions between the CO_2 gas and rock are presumable through its dissolution in brine as a ubiquitous fluid phase. Either the reduction in the pressure or the increase in the temperature leads to CO_2 escaping from the dissolution. It was considered that the concentration of CO_2 in brine is obtained from the equilibrium with brine at a pressure in the range between 1 MPa and the fluid pressure, p_f, at that depth. The pH value decreases with increasing equilibrium pressure. This section investigates the effect of CO_2 concentration (or pH) of CO_2-bearing fluids on the durability of the ITZs and the cement sheath. The CO_2 concentration in brine is calculated using the method developed by Duan and Sun (2003). Subsequently, the pH value is obtained based on the CO_2 concentration using the CrunchFlow code [81]. The calculations illustrate that at an equilibrium pressure of 1 MPa and a depth of 1650 m, the pH is 3.24. The pH level decreases to 2.88 with increasing the equilibrium pressure to the fluid pressure of 16.17 MPa at a depth of 1650 m. These two bounds of pH (2.88-3.24) do not show a significant change with depth. Therefore, the maximum change in the pH, $(\Delta pH)_{max}$, is around 0.36. ΔpH can be written as follows:

$$\Delta pH = pH_d - pH_{min} \quad (24)$$

where, pH_d and pH_{min} indicate the pH at the depth of d and the minimum pH value obtained at that depth with considering an equilibrium pressure of 1 MPa, respectively.

5.6.1 Injection wells

In injection wells, the cement sheath maintains its integrity for at least 2907 years. The cr is compacted over the entire range of the pH and all depths. The anticipated time for the occurrence of PDB at the cr, and CSB and DSB at the cc is beyond thousands of years. Figure 12 demonstrates that at any time after CO_2 injection commences, at least one of the cc or cr will fail due to the tensile or the shear stresses, respectively.

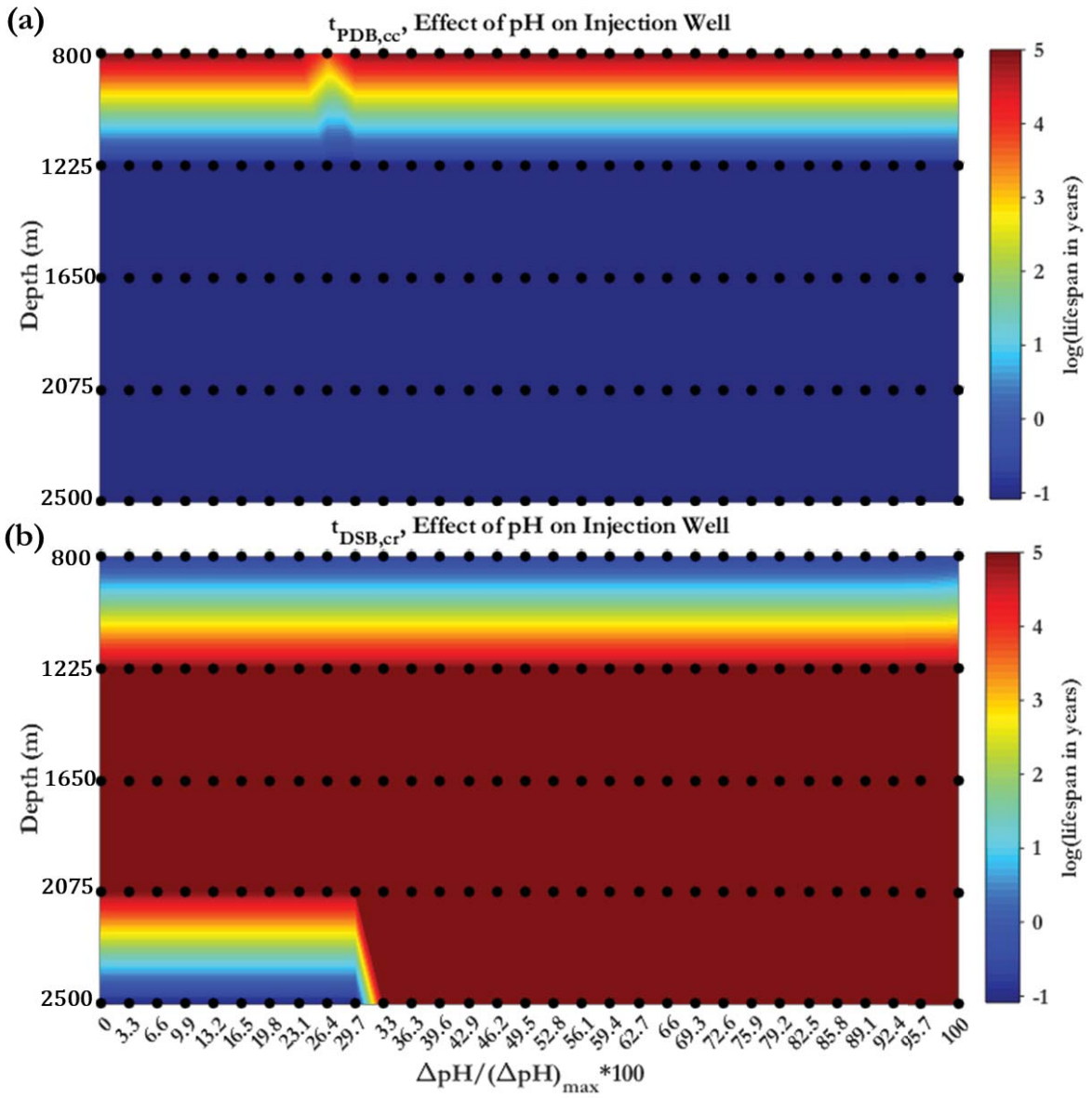

Figure 12. The failure time of (a) the cement-casing interfacial transition zone due to the tensile stress; and (b) the cement-rock interfacial transition zone due to the shear stress at different pH degrees.

5.6.2 Abandoned wells

The cr is also compacted in abandoned wells over the entire range of pH and depth. None of the ITZs and the cement sheath are predicted to fail in less than 2450 years.

5.7 Rocks

The rocks surrounding the cement sheath affect the degree of acidity of the CO_2-bearing fluids and transport mechanisms of carbon species into/out of the cement sheath. Two rock types of sandstone and limestone are investigated in this section. The main differences between them is assumed to be the composition and the maximum uniform confining stress which is bearable by them [54] defined as follows:

$$X_{sandstone} = 3663.85\exp(-12.4\phi) \quad (25)$$

$$X_{limestone} = 601.6\exp(-8.3\phi) \quad (26)$$

where, ϕ is porosity, $X_{sandstone}$ and $X_{limestone}$ indicate the maximum uniform confining stress which is bearable by sandstone and limestone, respectively. The uniaxial compressive strength of them are calculated as follows [82]:

$$f_c = 2.28 + 4.1089E \quad (27)$$

where E is the Young's modulus. This equation has been developed basically for sandstones. To simplify the comparison, Eq (27) is also applied to calculate the UCS of limestone rocks. In fact, the UCS of these rocks overlaps each other within an extensive area of the Young's modulus, E. The minimum value of the Young's modulus obtained as:

$$E_{min} = (\sigma_v - 2.28)/4.1089 \quad (28)$$

where, E_{min} is the minimum Young's modulus, and σ_v is the lithostatic stress calculated as follows [79]:

$$\sigma_v = 0.027d \quad (29)$$

For calculating E_{min}, it is assumed that the rock must be as strong as to withstand the lithostatic stress. The maximum Young's modulus, E_{max}, is assumed to be 57.85 GPa for a rock with UCS of 240 MPa derived from Eq. (27). Therefore, $(\Delta E)_{max}$ and ΔE can be expressed as:

$$(\Delta E)_{max} = E_{max} - E_{min} \quad (30)$$

$$\Delta E = E - E_{min} \quad (31)$$

5.7.1 Limestone

Limestone is a carbonate sedimentary rock in which many oil and gas reservoirs are located. Calcium carbonate is the main composing mineral of this rock type. The pH level of CO_2-bearing fluids in these rocks increases due to the dissolution of calcium carbonate. Equation (26) indicates that the limestone rocks are more susceptible to the deformation process.

5.7.1.1 Injection wells

Figure 13 shows that at the depth of 800 m and for $(\Delta E)_{max}/\Delta E$ less than 33% the cr and the cc will remain safe. At $(\Delta E)_{max}/\Delta E$ greater than or equal to 33% and the depth of 800 m the cr fails due to either the formation of PDB or DSB. As can be observed in Figure 13 (a), the cc fails at locations deeper than 800 m. Therefore, either the cc or the cr will fail except at the depth of 800 m and for $(\Delta E)_{max}/\Delta E$ less than 33%. The cr is compacted in a short time after the start of the CO_2 injection at all depths and for all the values of the Young's modulus, E. Figure 14 is an example that shows the change in the deformation criterion, η_d, for an injection well in a limestone formation at the Young's moduli of 10.29 and 57.85 GPa within a five-year time period. It is predicted that the cement sheath will not fail in a time period of less than 3726 years.

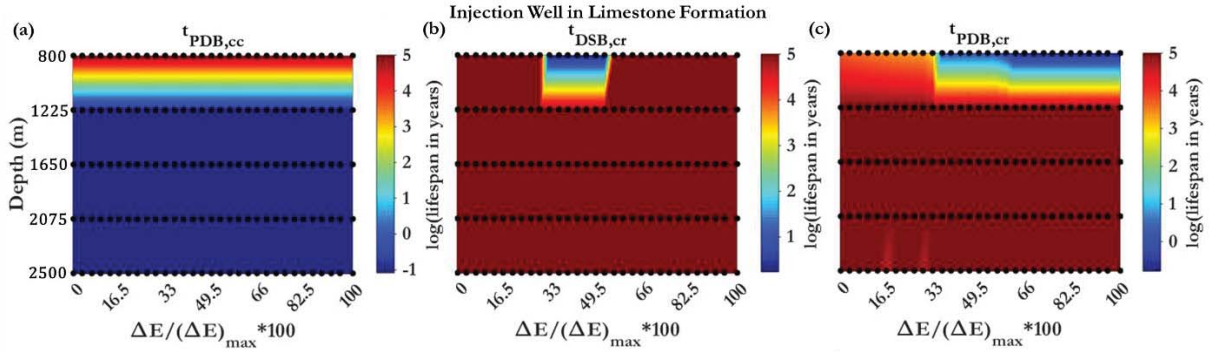

Figure 13. The failure of (a) the cc due to the tensile stress; (b) the cr due to the shear stress; (c) the cr due to tensile stress for an injection well in a limestone formation.

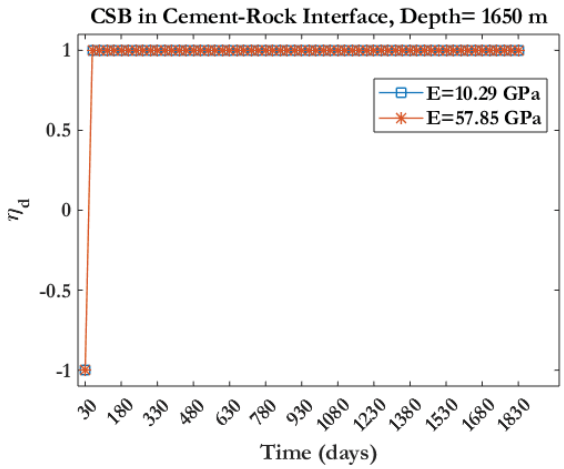

Figure 14. The evolution of the deformation criterion, η_d, for an injection well in a limestone formation at the Young's moduli of 10.29 and 57.85 GPa within a five-year time period.

5.7.1.2 Abandoned wells

The rock-cement-casing will remain safe in an abandoned well. The cr will be compacted due to the deformation process, as shown in Figure 15 (a). The tendency of the cement sheath to become dilated due to the shear stress as the succeeding process is shown in Figure 15 (b). This figure indicates that the cement sheath retains its integrity for more than 3199 years.

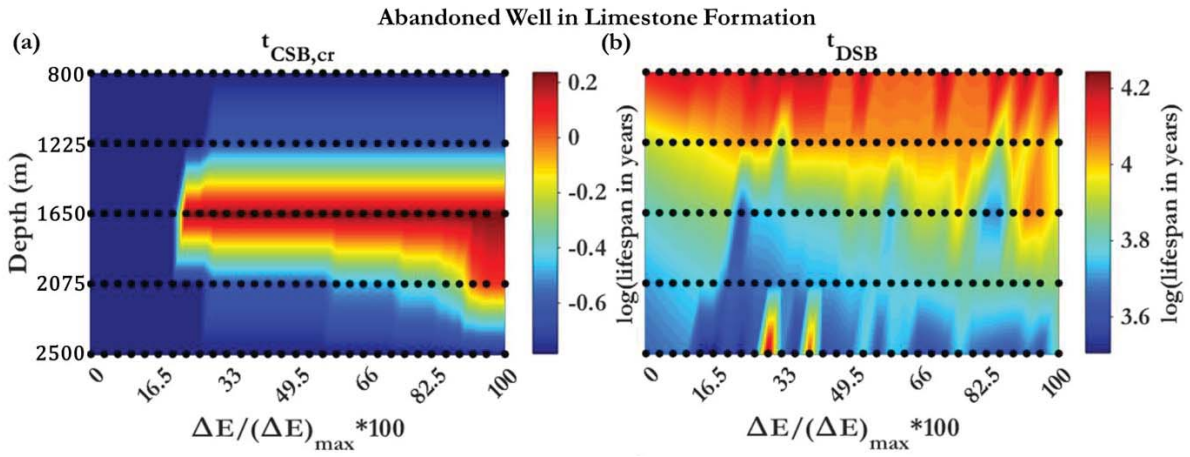

Figure 15. (a) The deformation time of the cement-rock interfacial transition zone; (b) the failure time of the cement sheath for an abandoned well in a limestone formation.

5.7.2 Sandstone

Sandstones are one of the common clastic sedimentary rocks that has a significant contribution to hydrocarbon reservoirs. They are mostly composed of silicates (SiO_2). CO_2-bearing fluids are rarely impacted by sandstone. In fact, the degree of acidity of CO_2-bearing fluids approximately remains intact and its initial composition prolongs for far longer than when it is exposed to limestone rocks. As can be inferred from Eq. (25), the deformation process is less likely to occur in sandstones. This justifies the brittleness behaviour of sandstones.

5.7.2.1 Injection wells

Either the cr or cc will fail in injection wells in sandstone formations, except at the depth of 800 m and in $(\Delta E)_{max}/\Delta E$ less than 33% as shown in Figure 16. The cr fails due to the shear stress with increasing in the Young's modulus. The cc remains intact at the depth of 800 m while it fails due to tensile stress at deeper locations. This is due to an increase in the temperature reduction at deeper depths. The cr is compacted in the first few days and the cement sheath shows an indefinite lifespan.

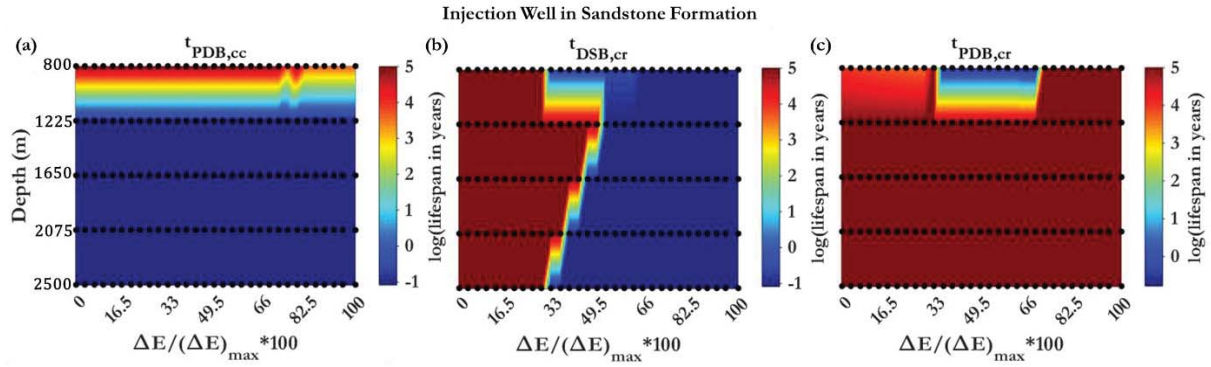

Figure 16. The failure of (a) the cc due to the tensile stress; (b) the cr due to the shear stress; (c) the cr due to tensile stress for an injection well in a sandstone formation.

5.7.2.2 *Abandoned wells*

For abandoned wells in sandstone formations, the cr in the rock-cement-casing assemblage is only affected by the stress state. The *in-situ* horizontal stress deforms (or compacts) the cr. This phenomenon increases the strength of the cr by reducing the porosity.

5.8 Prediction methodology

In the cases studied in this paper, the alteration of the rock-cement-casing assemblage was simulated over a five-year time period. 2,227 simulation cases were run to evaluate the effect of predefined parameters on the wellbore integrity. Consequently, conducting the model to simulate the behaviour beyond five years is a time-consuming and computationally expensive process. In addition, as observed in some cases, the failure time is predicted to be over thousands years. This means that the effect of the cumulative truncation and the round-off errors will bias the numerical trends. Therefore, to provide a comprehensive parametric study, a five-year time period was chosen for the simulations. The performance of the ITZs and the cement sheath were extrapolated based on the best fitted linear model to calculate their lifespan. As an example, the performance of the cement sheath under the shear stress within the first five years is shown in Figure 17 (a)-(c). The linear extrapolation predicts that the cement sheath will prolong for a minimum of 3714 years. Nevertheless, Figure 17 (a)-(c) not only confirm the validity of the extrapolated lifespans but also show that the cement sheath maintains its integrity longer than predicted by the extrapolation technique. This issue can be observed in the changing trends towards either the lower or constant values in a 50-year time period in Figure 17 (d)-(f).

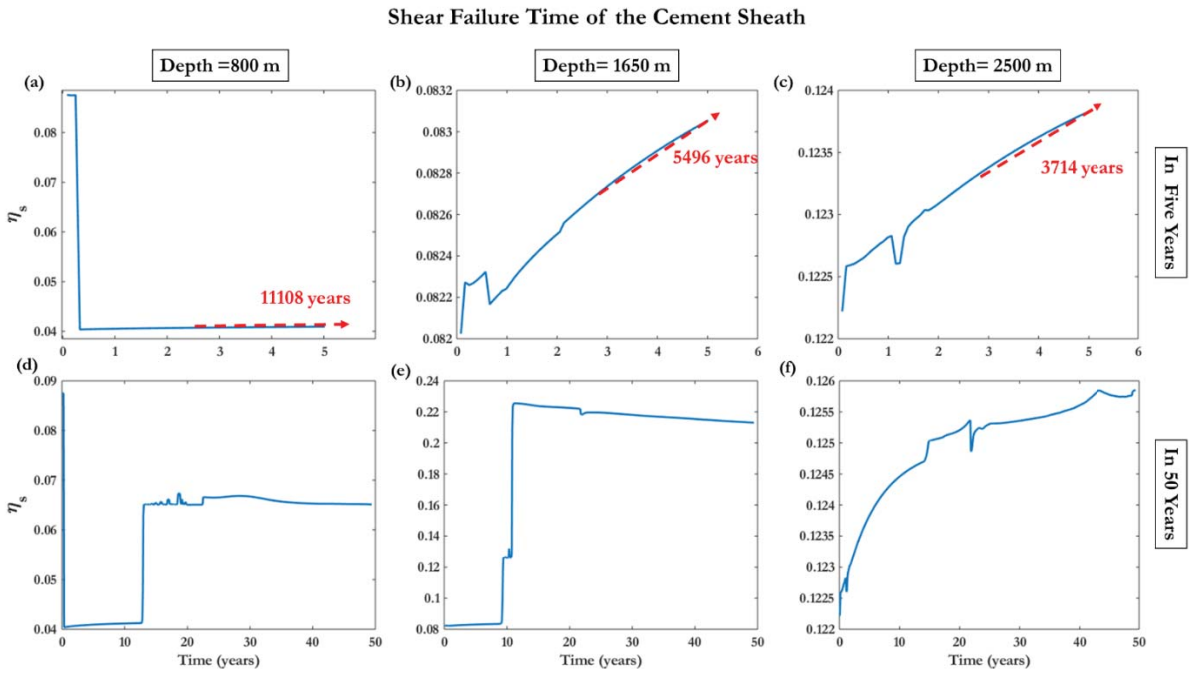

Figure 17. The shear failure time of the cement sheath for an injection well which abandoned after 2.5 years of being used for CO_2 injection, the performance of the cement sheath within the first five years at the depths of (a) 800, (b) 1650, and (c) 2500 m; and the first 50 years at the depths of (d) 800, (e) 1650, and (f) 2500 m.

6 Summary and conclusion

This paper provides a parametric study on wellbore integrity at different conditions found in CO_2 storage sites of hydrocarbon reservoirs. The model developed in [74] is used to investigate the performance of the rock-cement-casing assemblage in both injection and abandoned wells.

Table 5. The summary of the parametric study on the wellbore integrity (the values and bounds are provided in this table are estimations of what discussed in each section. Please, refer to the corresponding sections for more details).

Investigated parameter	Cement-casing interfacial transition zone	Cement-rock interfacial transition zone	Cement sheath
Temperature (it is only investigated in injection wells)	PDB generally forms at $\Delta T_w/(\Delta T)_{max}$ greater than or equal to 50% and at depths deeper than 1140 m during the first days after starting CO_2 injection.	DSB approximately forms at $\Delta T_w/(\Delta T)_{max}$ greater than or equal to 25%. The maximum bound for the formation of DSB is 100% for $\Delta T_w/(\Delta T)_{max}$ at the depth of 800 m while this bound decreases to about 60% at the depth of 2500 m during the first days after starting CO_2 injection. PDB almost forms at the range of 45-60% for $\Delta T_w/(\Delta T)_{max}$ when T_e is constant. This range changes to 90-100% when T_w is constant during the first days after starting CO_2 injection. It is fully compacted during the first days after starting CO_2 injection.	It remains safe. The minimum lifespan is 1897 years predicted for the cement sheath under the impact of the shear stress.
Composition and porosity in Injection wells	Early dilation at depths of 1650 and 2500 m.	DSB occurs under the following circumstances during the first days after starting CO_2 injection: 1- At the depth of 800 m, for all values of ϕ and x_{CH} except at ϕ of 0.05 and $x_{CH} \geq 25\%$. 2- At the depth of 1650 m, for $0.20 \leq \phi \leq 0.25$ and $15\% \leq x_{CH} \leq 20\%$. 3- At the depth of 2500 m, the approximate range is $0.15 \leq \phi \leq 0.25$ and $15\% \leq x_{CH} \leq 25\%$. The approximate zone for the formation of PDB is $0.15 < \phi \leq 0.25$ and $15\% \leq x_{CH} \leq 35\%$ at the depth of 800 m, while at the depths of 1650 and 2500 m it will retain its integrity for 494 and 10^5 years, respectively. It is fully compacted at all depths during the first days after starting CO_2 injection.	The minimum lifespan is 663 years predicted for the cement sheath if DSB forms at the depth of 1650 m. Therefore, the cement sheath retains its integrity for a long period of time.
Composition and porosity in abandoned wells	The minimum lifespan is 1628 years predicted for the formation of PDB at the depth of 1650 m.	The minimum lifespan is 1775 years predicted if PDB forms at the depth of 800 m. It is fully compacted at all depths very early during the first days after exposure to CO_2-bearing fluids.	The minimum lifespan is 2178 years predicted for the cement sheath if PDB forms at the depth of 2500 m. This means that the cement sheath at least remains safe for two thousand years.

***In-situ* horizontal stress in Injection wells**	PDB forms at wells deeper than 800 m.	DSB occurs under the following circumstances: 1- At the depth of 800 m. 2- Approximately at the depths between 1650-2500 m, and for $\Delta\sigma_{in-situ}/(\Delta\sigma_{in-situ})_{max}$ in the range of 0-10%. It is fully compacted at all depths and all the values of the *in-situ* horizontal stress once CO_2 injection is started.	None of DSB, PDB, and CSB are predicted to impact the cement sheath in a time period less than three thousand years.
***In-situ* horizontal stress in abandoned wells**	The formation of CSB approximately at $\Delta\sigma_{in-situ}/(\Delta\sigma_{in-situ})_{max}$ in the range of 60-100% and at the locations deeper than 1225 m during the first few days after exposure to CO_2-bearing fluids.	It is early compacted at all depths and all values of $\Delta\sigma_{in-situ}/(\Delta\sigma_{in-situ})_{max}$.	It will be compacted at the depth of 2500 m and $\Delta\sigma_{in-situ}/(\Delta\sigma_{in-situ})_{max}$ of 100%, 104 years after being exposed to CO_2-bearing fluids. The lifespan of the cement sheath increases to 10^5 at the loci of $\Delta\sigma_{in-situ}/(\Delta\sigma_{in-situ})_{max} = 0$ and the depth of 800 m.
Fluid pressure (it is only investigated in injection wells)	PDB forms at wells deeper than 800 m once CO_2 injection project is started.	DSB forms at depths of 800 m and 2500 m for all values of p_f once CO_2 is injected. At the same time scale, DSB will also be formed at the depth of 2075 m and for $\Delta p_f/(\Delta p_f)_{max}$ greater than 60%. It is compacted at all depths and all the values of the fluid pressure during the first few days after staring CO_2 injection.	None of DSB, PDB, and CSB are predicted to impact the cement sheath in less than three thousand years.
The thickness of the cement sheath in injection wells	PDB forms at wells deeper than 800 m once CO_2 injection project is started.	DSB forms at depths of 800 m and t/r in the range of 0.07-2.44 once CO_2 is injected. It is compacted at all depths and all the values of the cement sheath thickness during the first few days after staring CO_2 injection.	None of DSB, PDB, and CSB are predicted to impact the cement sheath in three thousand years.
The thickness of the cement sheath in abandoned wells	It will remain safe for at least one thousand years, and then PDB will form.	It is compacted at all depths and all the values of the cement sheath thickness during the first few days after exposure to CO_2-bearing fluids.	It will remain safe for at least one thousand years, and then PDB will form.
pH in injection wells	PDB forms at wells deeper than 800 m once CO_2 injection project is started.	Early formation of DSB at the depth of 800 m for the entire range of pH, at the depth of 2500 m for $\Delta pH/(\Delta pH)_{max}$ in the range of 0-29.7%. It is compacted at all depths and all the values pH during the first few days after staring CO_2 injection.	It will remain safe for 2907 years, and then DSB will form.
pH in abandoned wells	It will remain intact for 2450 years, and then PDB will form.	It keeps its integrity for 3555 years, and then PDB will form. It is compacted at all depths and all the values pH after being exposed to CO_2-bearing fluids.	It will remain safe for 3932 years, and then DSB will form.
Rocks: limestone surrounding injection wells	PDB forms at wells deeper than 800 m once CO_2 injection project is started.	The formation of DSB at depth of 800 m, and $\Delta E/(\Delta E)_{max}$ in the range of 33-51% during the first few days after staring CO_2 injection. The formation of PDB at $\Delta E/(\Delta E)_{max}$ greater than 33% at the depth of 800 m during the	It will fail after 3726 years due to the shear stress. The CSB is expected to deform the cement sheath after 3265 years.

		first few days after staring CO_2 injection. It is compacted at all depths and all the values E during the first few days after staring CO_2 injection.	
Rocks: limestone surrounding abandoned wells	It will collapse due to the tensile stress 1318 years after exposure to CO_2-bearing fluids.	It is compacted at all depths and all the values E after being exposed to CO_2-bearing fluids.	It will fail after 3199 years, and then DSB will form.
Rocks: sandstone surrounding injection wells	PDB forms at wells deeper than 800 m once CO_2 injection project is started.	The formation of DSB approximately at $\Delta E/(\Delta E)_{max}$ greater than 42% and all depths during the first few days after staring CO_2 injection. The formation of PDB at $\Delta E/(\Delta E)_{max}$ in the range of 36-69% at the depth of 800 m during the first few days after staring CO_2 injection.	The cement sheath will fail due to the shear stress 2886 years after staring CO_2 injection.
Rocks: sandstone surrounding abandoned wells	The formation of DSB at the cc place after 2305 years.	It is compacted during the first few days after exposure to CO_2-bearing fluids at all depths and the Young moduli.	The CSB is expected to deform the entire cement sheath 2618 years after exposure to CO_2-bearing fluids. It will also fail after 2781 years due to the shear stress.

As can be understood from Table 5, either the failure of the cc or cr is inevitable in injection wells. Although the failure at the cr in the injection wells is less likely to occur than in cc locations, it would be more detrimental. In fact, the cr failure directly provides the leakage pathway for CO_2-bearing fluids to shallower depths while CO_2-bearing fluids must pass through the cement sheath to reach the gap between the cement and its casing. Table 5 indicates that the deformation of the cr is expected under all conditions found in CO_2 storage sites. In addition, the carbonation process reduces the porosity and increases the strength of the calcite precipitation zones close to the cement-rock interface. These aforementioned reasons are enough to narrow the chance of CO_2-bearing fluids breaking through the cement sheath towards the cement-casing interface. Nevertheless, the low permeability of the cement sheath itself limits the fluid permeation. Abandoned wells show that they are completely under the impact of the deformation process, and none of DSB and PDBs are expected to disintegrate them within the first thousand years after exposure to CO_2-bearing fluids.

Both Injection and abandoned wells are subject to the compaction forces prior to the commencement of CO_2-injection and exposure to CO_2-bearing fluids, respectively. Therefore, although their activity were observed in the simulations in this paper, actually they have been acting on the rock-cement-casing assemblage since the establishment of the wellbores. Overall, the cement sheath, in both injection and abandoned wells, is seen to retain its integrity for the minimum of one thousand years. It is worth noting that the compaction of the cr and the extremely low permeability of the cement sheath also help in prolonging its lifetime.

Acknowledgements

We would like to offer our special thanks to the Research Centre for Fluid and Complex Systems (FCS) and the Research Centre for Built and Natural Environment (BNE) at Coventry

University for their financial support. We would also like to express our very great appreciation to the staff at these two centres for supporting this work through their invaluable comments. We wish to acknowledge the help of Dr Philip Costen provided us with constructive comments on improving the manuscript. We also thank Dr Carl Steefel for providing the CrunchFlow code.

Nomenclature

Acronyms	**Full Name**
cc	Casing-cement interfacial transition zone
CCS	Carbon capture and storage
CH	Portlandite
CSB	Compaction shear bands
C-S-H	Calcium silicate hydrate
cr	Cement-rock interfacial transitional zone
DSB	Dilation shear bands
PDB	Pure dilation shear bands
UCS	Uniaxial compressive strength

Appendix A

A.1 Tensile failure

The tensile failure can be characterised as follows [50,51]:

$$M = \min\{\sigma_r, \sigma_\theta, \sigma_z\} - \alpha p \quad \text{A. 1}$$

then,

$$\eta_t = -\frac{M}{f_t} \quad \text{A. 2}$$

The rock will fail under the tensile stress if the value of η_t as the tensile failure criterion becomes greater than one.

A.2 Shear failure

The Drucker-Prager criterion [53] can be written as:

$$\tau_{DP} = \tau_0 + m(\sigma_{oct} - \alpha p) \quad \text{A. 3}$$

where, τ_{DP} is the Drucker-Prager shear stress, which is the maximum shear stress that can be withstood by a rock, τ_0 and m are the intercept and slope of the Drucker-Prager criterion, respectively, depending on the internal friction angle, φ, and the cohesion, C, of a rock as follows [51]:

$$\tau_0 = \frac{2\sqrt{2}Ccos\varphi}{3 - sin\varphi} \quad \text{A. 4}$$

$$m = \frac{2\sqrt{2}sin\varphi}{3 - sin\varphi} \quad \text{A. 5}$$

The internal friction angle, φ, and the cohesion, C, of a rock can be written as functions of compressive strength, f_c, as follows [83]:

$$\varphi = \sin^{-1}\left(\frac{3}{1 + 0.4f_c/\sqrt{3}}\right) \quad \text{A. 6}$$

$$c = (f_c - 5\sqrt{3})\frac{3 - sin\varphi}{6cos\varphi} \quad \text{A. 7}$$

Octahedral normal stress, σ_{oct}, and octahedral shear stress, τ_{oct}, are defined as:

$$\sigma_{oct} = \frac{I_1}{3} \quad \text{A. 8}$$

$$\tau_{oct} = \sqrt{\frac{2}{3}J_2} \quad \text{A. 9}$$

where, I_1 and J_2 are the first invariant of the stress tensor and the second invariant of the deviatoric stress tensor defined as follows:

$$I_1 = \sigma_r + \sigma_\theta + \sigma_z \quad \text{A. 10}$$

$$J_2 = \frac{1}{6}((\sigma_r - \sigma_\theta)^2 + (\sigma_r - \sigma_z)^2 + (\sigma_\theta - \sigma_z)^2) + \tau_{r\theta}^2 + \tau_{rz}^2 + \tau_{\theta z}^2 \quad \text{A. 11}$$

$\tau_{r\theta}$, τ_{rz}, and $\tau_{\theta z}$ are the shear stresses which are equal to zero due to the plane strain assumption and the symmetry of the cylindrical coordinate system which has been applied to demonstrate the rock-cement-casing assemblage.

Therefore, the shear failure criterion is as follows:

$$\eta_s = \frac{\tau_{oct}}{\tau_{DP}} \quad \text{A. 12}$$

The rock will take a shear failure if the shear failure criterion, η_s, increases to greater than one.

A.3 Deformation

A cap surface describes the boundary of the elastic-compaction areas which is characterised by using an elliptical equation as follows [54–58]:

$$\frac{(I_1{}' - c)^2}{a^2} + \frac{J_{2cap}}{b^2} - 1 = 0 \quad \text{A. 13}$$

where, I_1' is the effective first invariant of the stress tensor which is equal to $(I_1 - 3\alpha p)$ and J_{2cap} is the second invariant of the deviatoric stress tensor at the cap surface locus. The deformation criterion can be defined as:

$$\eta_d = \begin{cases} \dfrac{J_2}{J_{2cap}} & c \le I_1 < (c + a) \\ \dfrac{I_1}{a} & I_1 \ge (c + a) \end{cases} \quad \text{A. 14}$$

The values for a, b, and c are obtained after some mathematical manipulation as follows, for the cement matrix [58]

$$X_2 = 17.087 + 1.892f_{c,cement} \quad \text{A. 15}$$

$$X_2 = c + a \quad \text{A. 16}$$

$$r = 4.45994 \exp\left(\frac{-f_{c,cement}}{11.51679}\right) + 1.95358 \quad \text{A. 17}$$

$$\alpha_1 = \sqrt{\frac{3}{2}}\tau_0 \quad \text{A. 18}$$

$$\alpha_2 = \frac{m}{\sqrt{6}} \quad \text{A. 19}$$

where, $f_{c,cement}$ is the uniaxial compressive strength of the cement matrix. Therefore, the value of c for the cement matrix is:

$$c = \frac{X_2 - r\alpha_1}{1 + r\alpha_2} \quad \text{A. 20}$$

For the sandstone [54]

$$X_2 = 3 * X_{sandstone} \quad \text{A. 21}$$

$$mc = 2\phi + 0.882 \quad \text{A. 22}$$

And the value of c for the sandstone is:

$$c = \frac{X_2}{1 + \left(\frac{0.805}{mc}\right)^2} + 3\alpha p \quad \text{A. 23}$$

And for the limestone [54] after some mathematical manipulation

$$X_2 = 3 * X_{limestone} \quad \text{A. 24}$$

$$c' = 40.3\exp(-5.4\phi) \quad \text{A. 25}$$

$$\phi' = -89.3\phi + 49.0 \quad \text{A. 26}$$

$$A' = 6c' \cos(\phi') / (3 - \sin(\phi')) \quad \text{A. 27}$$

$$B' = 6 \sin(\phi') / (3 - \sin(\phi')) \quad \text{A. 28}$$

$$a_q = B'^2 + 1 \quad \text{A. 29}$$

$$b_q = 2A'B' \quad \text{A. 30}$$

$$c_q = A'^2 - \left(\frac{X_2}{3}\right)^2 \quad \text{A. 31}$$

$$c = 3(\alpha p + \left(-b_q + \sqrt{b_q^2 - 4a_q c_q}\right))/(2a_q) \quad \text{A. 32}$$

The values of a and b for both the cement matrix and the sandstone/limestone can be calculated as follows:

$$a = X_2 - c \quad \text{A. 33}$$

$$b = \alpha_1 + \alpha_2 c \quad \text{A. 34}$$

Appendix B

Table A. 1 Young's modulus, Poisson's ratio, density, and coefficient of thermal expansion for the casing, cement, and rock.

Component composing the solid phase of the cement matrix	**Young's modulus (GPa)**	**Reference**	**Density (gr/cm^3), the values are obtained from the CrunchFlow database** [71]
C-S-H	25.55	An average value is derived from [84–86]	2.24
CH	38.5	An average value is derived from [84,87]	2.71
Calcite	70	An average value is derived from [88]	2.05
Silica gel	159	It is assumed that the silica gel zone is composed of silicon and an average value is derived from [89,90]	2.07
Halite	3	[91]	2.16
Poisson's ratio, ν			
Poisson's ratio		**Reference**	
Poisson's ratio of cement matrix, ν_{cement}	0.25	[84,87,92–94]	
Poisson's ratio of rock, ν_{rock}	0.21	[37]	
Poisson's ratio of casing, ν_{casing}	0.27	[36,37]	
Young's modulus of rock and casing			
Young's modulus (GPa)		**Reference**	
The initial Young's modulus for Rock, $E_{0,rock}$	30	[37]	
Young's modulus of	205.6	[36,37]	

casing, E_{casing}		
Coefficient of thermal expansion, α_{CTE}		
Coefficient of thermal expansion ($1/℃$)		**Reference**
Coefficient of thermal expansion of cement, $\alpha_{CTE,cement}$	15e-6	[95,96]
Coefficient of thermal expansion of rock, $\alpha_{CTE,rock}$	10.8e-6	[37,95,97]
Coefficient of thermal expansion of casing, $\alpha_{CTE,casing}$	13e-6	[42,95]

The Voigt model is chosen to calculate the Young's modulus of the cement matrix. This is based on the direct effect of the geochemical reactions on the strength and the Young's modulus of a cement matrix [4,5]. Therefore, the Young's modulus for a cement matrix at a time, t, and a radius, r, from the centre of the cement sheath with assuming a porosity of zero can be written as follows:

$$E_{0,r}^{t} = \sum_{i=1}^{N_m} E_i f_{i,r}^{t} \qquad A.\ 35$$

where, $E_{0,r}^{t}$ is the Young's modulus of the cement matrix with a porosity of zero at the time, t, and the radius, r, E_i is the Young's modulus for the mineral i, $f_{i,r}^{t}$ shows the volume fraction of the mineral i over the entire volume of the solid phase, and N_m is the number of minerals in the cement matrix. It is worth noting that, in this paper, the materials which are formed or dissolved during the exposure to CO_2-bearing fluids are limited to the materials which are mentioned in Table A. 1. $f_{i,r}^{t}$ is also a function of the time, t, and the radius, r, due to the alteration in the cement composition during exposure to CO_2-bearing fluids. With increasing porosity the Young's modulus of the cement matrix decreases, and the following equation is suggested to consider the effect of porosity [98]:

$$E_r^t = E_{0,r}^{t}(1 - a\phi_r^t)^{n_r^t} \qquad A.\ 36$$

E_r^t, ϕ_r^t, and n_r^t are the Young's modulus of the cement matrix, the porosity, and a material constant at the time, t, and the radius, r. The material constant, a, is assumed to be equal to one by considering the Young's modulus of zero at the porosity of one [99,100]. Eq. A. 36 is also applicable for the rock surrounding the cement sheath.

References

[1] T.F. Stocker, G.-K. Plattner, M.M.B. Tignor, S.K. Allen, J. Boschung, A. Nauels, Y. Xia, V. Bex, P.M. Midgley, Climate Change 2013, 2013. https://doi.org/10.1017/CBO9781107415324.Summary.

[2] J.T. Kiehl, K.E. Trenberth, Earth's Annual Global Mean Energy Budget, Bull. Am. Meteorol. Soc. 78 (1997) 5. https://doi.org/10.1175/1520-0477(1997)078<0197:EAGMEB>2.0.CO;2.

[3] T.L. Watson, S. Bachu, Evaluation of the Potential for Gas and CO2 Leakage Along Wellbores, E&P Environ. Saf. Conf. (2009) 115–126. https://doi.org/10.2118/106817-MS.

[4] M. Bagheri, S.M. Shariatipour, E. Ganjian, A Study on the Chemo-mechanical Alteration of Cement in CO2 Storage Sites, SPE Eur. Featur. 81st EAGE Annu. Conf. Exhib. SPE-195520 (2019).

[5] M. Bagheri, S.M. Shariatipour, E. Ganjian, Prediction of the lifespan of cement at a specific depth based on the coupling of geomechanical and geochemical processes for CO2 storage, Int. J. Greenh. Gas Control. 86 (2019) 43–65. https://doi.org/10.1016/j.ijggc.2019.04.016.

[6] D.G. Calvert, D.K. Smith, O.K. Duncan, Issues and Techniques of Plugging and Abandonment of Oil and Gas Wells, 1994. https://www.onepetro.org/download/conference-paper/SPE-28349-MS?id=conference-paper%2FSPE-28349-MS (accessed January 24, 2019).

[7] M.A. Celia, S. Bachu, J.M. Nordbotten, D. Kavetski, S. Gasda, A risk assessment modeling tool to quantify leakage potential through wells in mature sedimentary basins, Proc. 8th Int. Conf. Greenh. Gas Control Technol. Trondheim, Norw. (2006) 1–6. http://scholar.google.com/scholar?hl=en&btnG=Search&q=intitle:A+risk+assessment+modeling+tool+to+quantify+leakage+potential+through+wells+in+mature+sedimentary+basins#0.

[8] R.J. Davies, S. Almond, R.S. Ward, R.B. Jackson, C. Adams, F. Worrall, L.G. Herringshaw, J.G. Gluyas, M.A. Whitehead, Oil and gas wells and their integrity: Implications for shale and unconventional resource exploitation, Mar. Pet. Geol. 56 (2014) 239–254. https://doi.org/10.1016/J.MARPETGEO.2014.03.001.

[9] M.U. Onoja, J.D.O. Williams, H. Vosper, S.M. Shariatipour, Effect of sedimentary heterogeneities in the sealing formation on predictive analysis of geological CO 2 storage, Int. J. Greenh. Gas Control. 82 (2019) 229–243. https://doi.org/10.1016/j.ijggc.2019.01.013.

[10] A.J. Newell, S.M. Shariatipour, Linking outcrop analogue with flow simulation to reduce uncertainty in sub-surface carbon capture and storage: an example from the Sherwood Sandstone Group of the Wessex Basin, UK, Geol. Soc. London, Spec. Publ. 436 (2016) 231 LP – 246. https://doi.org/10.1144/SP436.2.

[11] S.M. Shariatipour, G.E. Pickup, E.J. Mackay, Simulations of CO2 storage in aquifer

models with top surface morphology and transition zones, Int. J. Greenh. Gas Control. 54 (2016) 117–128. https://doi.org/10.1016/J.IJGGC.2016.06.016.

[12] M. Ahmadinia, S.M. Shariatipour, O. Andersen, M. Sadri, Benchmarking of vertically integrated models for the study of the impact of caprock morphology on CO2 migration, Int. J. Greenh. Gas Control. 90 (2019) 102802. https://doi.org/10.1016/j.ijggc.2019.102802.

[13] S.M. Shariatipour, G.E. Pickup, E.J. Mackay, Investigation of CO2 storage in a saline formation with an angular unconformity at the caprock interface, Pet. Geosci. 22 (2016) 203–210. https://doi.org/10.1144/petgeo2015-039.

[14] M. Bagheri, S.M. Shariatipour, E. Ganjian, A review of oil well cement alteration in CO2-rich environments, Constr. Build. Mater. 186C (2018) 946–968. https://doi.org/10.1016/j.conbuildmat.2018.07.250.

[15] H. Abdoulghafour, P. Gouze, L. Luquot, R. Leprovost, Characterization and modeling of the alteration of fractured class-G Portland cement during flow of CO2-rich brine, Int. J. Greenh. Gas Control. 48 (2016) 155–170. https://doi.org/10.1016/j.ijggc.2016.01.032.

[16] C. Geloni, T. Giorgis, A. Battistelli, Modeling of Rocks and Cement Alteration due to CO2Injection in an Exploited Gas Reservoir, Transp. Porous Media. 90 (2011) 183–200. https://doi.org/10.1007/s11242-011-9714-0.

[17] N.J. Huerta, M.A. Hesse, S.L. Bryant, B.R. Strazisar, C. Lopano, CO2-saturated water in a cement fracture : Application to wellbore leakage during geologic CO2 storage, 44 (2016) 276–289.

[18] B.M. Huet, J.H. Prevost, G.W. Scherer, Quantitative reactive transport modeling of Portland cement in CO2-saturated water, Int. J. Greenh. Gas Control. 4 (2010) 561–574. https://doi.org/10.1016/j.ijggc.2009.11.003.

[19] J. Shen, P. Dangla, M. Thiery, Reactive transport modeling of CO2 through cementitious materials under CO2 geological storage conditions, Int. J. Greenh. Gas Control. 18 (2013) 75–87. https://doi.org/10.1016/j.ijggc.2013.07.003.

[20] J.P.L. Brunet, L. Li, Z.T. Karpyn, N.J. Huerta, Fracture opening or self-sealing: Critical residence time as a unifying parameter for cement-CO2-brine interactions, Int. J. Greenh. Gas Control. 47 (2016) 25–37. https://doi.org/10.1016/j.ijggc.2016.01.024.

[21] B.G. Kutchko, B.R. Strazisar, N. Huerta, G. V. Lowry, D.A. Dzombak, N. Thaulow, CO2 reaction with hydrated class H well cement under geologic sequestration conditions: Effects of flyash admixtures, Environ. Sci. Technol. 43 (2009) 3947–3952. https://doi.org/10.1021/es803007e.

[22] W. Ashraf, Carbonation of cement-based materials: Challenges and opportunities, Constr. Build. Mater. 120 (2016) 558–570. https://doi.org/10.1016/j.conbuildmat.2016.05.080.

[23] K. Nakano, A. Ohbuchi, S. Mito, Z. Xue, Chemical interaction of well composite samples with supercritical CO2 along the cement - Sandstone interface, Energy Procedia. 63 (2014) 5754–5761. https://doi.org/10.1016/j.egypro.2014.11.608.

[24] A. Fabbri, J. Corvisier, A. Schubnel, F. Brunet, B. Goffé, G. Rimmele, V. Barlet-Gouédard, Effect of carbonation on the hydro-mechanical properties of Portland cements, Cem. Concr. Res. 39 (2009) 1156–1163. https://doi.org/10.1016/j.cemconres.2009.07.028.

[25] V.G. Papadakis, C.G. Vayenas, M.N. Fardis, Experimental investigation and mathematical modeling of the concrete carbonation problem, Chem. Eng. Sci. 46 (1991) 1333–1338. https://doi.org/10.1016/0009-2509(91)85060-B.

[26] A. Rezagholilou, V.G. Papadakis, H. Nikraz, Rate of carbonation in cement modified base course material, Constr. Build. Mater. 150 (2017) 646–652. https://doi.org/10.1016/j.conbuildmat.2017.05.226.

[27] A. Duguid, G.W. Scherer, Degradation of oilwell cement due to exposure to carbonated brine, Int. J. Greenh. Gas Control. 4 (2010) 546–560. https://doi.org/10.1016/j.ijggc.2009.11.001.

[28] J.P.L. Brunet, L. Li, Z.T. Karpyn, B.G. Kutchko, B. Strazisar, G. Bromhal, Dynamic evolution of cement composition and transport properties under conditions relevant to geological carbon sequestration, Energy and Fuels. 27 (2013) 4208–4220. https://doi.org/10.1021/ef302023v.

[29] N.J. Huerta, S.L. Bryant, L. Conrad, Cement Core Experiments With A Conductive Leakage Pathway , Under Confining Stress And Alteration Of Cement ' s Mechanical Properties Via A Reactive Fluid , As An Analog For CO2 Leakage Scenario, SPE/DOE Improv. Oil Recover. Symp. Tulsa, Oklahoma, 19-23 April. SPE-113375 (2008). https://doi.org/10.2118/113375-MS.

[30] B.G. Kutchko, B.R. Strazisar, D.A. Dzombak, G. V Lowry, N. Thaulow, Degradation of Well Cement by CO2 under Geological Sequestration Conditions, Env. Sci Technol. 41 (2007) 4787–4792. https://doi.org/10.1021/es062828c.

[31] B. Lecampion, J. Vanzo, F.-J. Ulm, B. Huet, C. Germay, I. Khalfallah, J. Dirrenberger, Evolution of Portland Cement Mechanical Properties Exposed To Co2-Rich Fluids: Investigation At Different Scales, MPPS 2011, Symp. Mech. Phys. Porous Solids A Tribut. to Pr. Oliv. Coussy. (2011) 1–24.

[32] S.D.C. Walsh, H.E. Mason, W.L. Du Frane, S.A. Carroll, Mechanical and hydraulic coupling in cement-caprock interfaces exposed to carbonated brine, Int. J. Greenh. Gas Control. 25 (2014) 109–120. https://doi.org/10.1016/j.ijggc.2014.04.001.

[33] L. Zhang, D.A. Dzombak, D. V. Nakles, J.P.L. Brunet, L. Li, Reactive transport modeling of interactions between acid gas (CO 2 + H2S) and pozzolan-amended wellbore cement under geologic carbon sequestration conditions, Energy and Fuels. 27 (2013) 6921–6937. https://doi.org/10.1021/ef401749x.

[34] W. Wang, A.D. Taleghani, Three-dimensional analysis of cement sheath integrity around Wellbores, J. Pet. Sci. Eng. 121 (2014) 38–51. https://doi.org/10.1016/j.petrol.2014.05.024.

[35] E. Arjomand, T. Bennett, G.D. Nguyen, Evaluation of cement sheath integrity subject to enhanced pressure, J. Pet. Sci. Eng. 170 (2018) 1–13. https://doi.org/10.1016/j.petrol.2018.06.013.

[36] R. Gholami, V. Rasouli, B. Aadnoy, M. Mohammadnejad, Geomechanical and numerical studies of casing damages in a reservoir with solid production, Rock Mech. Rock Eng. 49 (2016) 1441–1460. https://doi.org/10.1007/s00603-015-0828-5.

[37] R. Gholami, B. Aadnoy, N. Fakhari, A thermo-poroelastic analytical approach to evaluate cement sheath integrity in deep vertical wells, J. Pet. Sci. Eng. 147 (2016) 536–546. https://doi.org/10.1016/j.petrol.2016.09.024.

[38] E. Hoek, E.T. Brown, Practical estimates of rock mass strength, Int. J. Rock Mech. Min. Sci. 34 (1997) 1165–1186. https://doi.org/10.1016/S1365-1609(97)80069-X.

[39] M.A. Biot, Theory of elasticity and consolidation for a porous anisotropic solid, J. Appl. Phys. 26 (1955) 182–185. https://doi.org/10.1063/1.1721956.

[40] V.I. Osipov, Physicochemical theory of effective stress in soils, Physicochem. Theory Eff. Stress Soils. (2015) 1–55. https://doi.org/10.1007/978-3-319-20639-4.

[41] A. Nur, J.D. Byerlee, An exact effective stress law for elastic deformation of rock with fluids, J. Geophys. Res. 76 (1971) 6414–6419. https://doi.org/10.1029/JB076i026p06414.

[42] M.H. Sadd, Elasticity. Theory, Applications, and Numerics, 2005.

[43] P. Maimí, P.P. Camanho, J.A. Mayugo, C.G. Dávila, A continuum damage model for composite laminates: Part I - Constitutive model, Mech. Mater. 39 (2007) 897–908. https://doi.org/10.1016/j.mechmat.2007.03.005.

[44] J. Lubliner, J. Oliver, S. Oller, E. Oñate, A plastic-damage model for concrete, Int. J. Solids Struct. 25 (1989) 299–326. https://doi.org/10.1016/0020-7683(89)90050-4.

[45] J. Lee, G.L. Fenves, Plastic-Damage Model for Cyclic Loading of Concrete Structures, J. Eng. Mech. 124 (1998) 892–900. https://doi.org/10.1061/(ASCE)0733-9399(1998)124:8(892).

[46] Y. Xiao, Z. Chen, J. Zhou, Y. Leng, R. Xia, Concrete plastic-damage factor for finite element analysis: Concept, simulation, and experiment, Adv. Mech. Eng. 9 (2017) 1–10. https://doi.org/10.1177/1687814017719642.

[47] H. Fossen, R. Soliva, G. Ballas, B. Trzaskos, C. Cavalcante, R.A. Schultz, A review of deformation bands in reservoir sandstones: geometries, mechanisms and distribution, Geol. Soc. London, Spec. Publ. 459 (2018) 9–33. https://doi.org/10.1144/sp459.4.

[48] H. Fossen, A. Bale, Deformation bands and their influence on fluid flow, Am. Assoc. Pet. Geol. Bull. 91 (2007) 1685–1700. https://doi.org/10.1306/07300706146.

[49] H. Fossen, R.A. Schultz, Z.K. Shipton, K. Mair, Deformation bands in sandstone: a review, J. Geol. Soc. London. 164 (2007) 755–769. https://doi.org/10.1144/0016-76492006-036.

[50] M.R. McLean, M.A. Addis, Wellbore Stability Analysis: A Review of Current Methods of Analysis and Their Field Application, SPE/IADC Drill. Conf. 27 February-2 March, Houston, Texas. (1990).

[51] M.R. McLean, M.A. Addis, Wellbore Stability: The Effect of Strength Criteria on Mud

Weight Recommendations, SPE Annu. Tech. Conf. Exhib. (1990). https://doi.org/10.2118/20405-MS.

[52] J. Zhao, Applicability of Mohr-Coulomb and Hoek-Brown strength criteria to the dynamic strength of brittle rock, Int. J. Rock Mech. Min. Sci. 37 (2000) 1115–1121. https://doi.org/10.1016/S1365-1609(00)00049-6.

[53] D.C. Drucker, W. Prager, SOIL MECHANICS AND PLASTIC ANALYSIS OR LIMIT DESIGN, Q. Appl. Math. 10 (1952) 157–165. https://pdfs.semanticscholar.org/6583/be285aef2087223d19e890c8d94aa8a89805.pdf (accessed November 8, 2018).

[54] E. Bemer, O. Vincké, P. Longuemare, Geomechanical log deduced from porosity and mineralogical content, Oil Gas Sci. Technol. 59 (2004) 405–426. https://doi.org/10.2516/ogst:2004028.

[55] V.A. Lubarda, S. Mastilovic, J. Knap, Brittle-Ductile Transition in Porous Rocks by Cap Model, J. Eng. Mech. 122 (1996) 633–642. https://doi.org/10.1061/(asce)0733-9399(1996)122:7(633).

[56] T. Wong, C. David, W. Zhu, The transition from brittle faulting to cataclastic flow in porous sandstones: Mechanical deformation, J. Geophys. Res. Solid Earth. 102 (1997) 3009–3025. https://doi.org/10.1029/96jb03281.

[57] W. Zhu, T. Wong, The transition from brittle faulting to cataclastic flow: Permeability evolution, J. Geophys. Res. Solid Earth. 102 (1997) 3027–3041. https://doi.org/10.1029/96jb03282.

[58] H. Jiang, J. Zhao, Calibration of the continuous surface cap model for concrete, Finite Elem. Anal. Des. 97 (2015) 1–19. https://doi.org/10.1016/j.finel.2014.12.002.

[59] K. Jurowski, S. Grzeszczyk, Influence of selected factors on the relationship between the dynamic elastic modulus and compressive strength of concrete, Materials (Basel). 11 (2018). https://doi.org/10.3390/ma11040477.

[60] D. Shen, X. Shi, S. Zhu, X. Duan, J. Zhang, Relationship between tensile Young's modulus and strength of fly ash high strength concrete at early age, Constr. Build. Mater. 123 (2016) 317–326. https://doi.org/10.1016/j.conbuildmat.2016.06.145.

[61] N. Arıoglu, Z.C. Girgin, E. Arıoglu, Evaluation of ratio between splitting tensile strength and compressive strength for concretes up to 120 MPa and its application in strength criterion, ACI Mater. J. 103 (2006) 18–24.

[62] A. Aydin, R.I. Borja, P. Eichhubl, Geological and mathematical framework for failure modes in granular rock, J. Struct. Geol. 28 (2006) 83–98. https://doi.org/10.1016/j.jsg.2005.07.008.

[63] H. Fossen, Geometric analysis and scaling relations of deformation bands in porous sandstone, 19 (1997).

[64] X. Du Bernard, P. Eichhubl, A. Aydin, Dilation bands: A new form of localized failure in granular media, Geophys. Res. Lett. 29 (2002) 29-1-29–4. https://doi.org/10.1029/2002gl015966.

[65] Y. Hamiel, V. Lyakhovsky, A. Agnon, Coupled evolution of damage and porosity in poroelastic media: Theory and applications to deformation of porous rocks, Geophys. J. Int. 156 (2004) 701–713. https://doi.org/10.1111/j.1365-246X.2004.02172.x.

[66] R.A. Schultz, R. Siddharthan, A general framework for the occurrence and faulting of deformation bands in porous granular rocks, Tectonophysics. 411 (2005) 1–18. https://doi.org/10.1016/j.tecto.2005.07.008.

[67] R.A. Schultz, R. Soliva, H. Fossen, C.H. Okubo, D.M. Reeves, Dependence of displacement-length scaling relations for fractures and deformation bands on the volumetric changes across them, J. Struct. Geol. 30 (2008) 1405–1411. https://doi.org/10.1016/j.jsg.2008.08.001.

[68] K. Abid, R. Gholami, P. Choate, B.H. Nagaratnam, A review on cement degradation under CO2-rich environment of sequestration projects, J. Nat. Gas Sci. Eng. 27 (2015) 1149–1157. https://doi.org/10.1016/j.jngse.2015.09.061.

[69] H.E. Mason, W.L. Du Frane, S.D.C. Walsh, Z. Dai, S. Charnvanichborikarn, S.A. Carroll, Chemical and mechanical properties of wellbore cement altered by CO 2-rich brine using a multianalytical approach, Environ. Sci. Technol. 47 (2013) 1745–1752. https://doi.org/10.1021/es3039906.

[70] A. Duguid, M. Radonjic, G.W. Scherer, Degradation of cement at the reservoir/cement interface from exposure to carbonated brine, Int. J. Greenh. Gas Control. 5 (2011) 1413–1428. https://doi.org/10.1016/j.ijggc.2011.06.007.

[71] C.I. Steefel, C.A.J. Appelo, B. Arora, D. Jacques, T. Kalbacher, O. Kolditz, V. Lagneau, P.C. Lichtner, K.U. Mayer, J.C.L. Meeussen, S. Molins, D. Moulton, H. Shao, J. Šimůnek, N. Spycher, S.B. Yabusaki, G.T. Yeh, Reactive transport codes for subsurface environmental simulation, 2015. https://doi.org/10.1007/s10596-014-9443-x.

[72] H. Xu, T. Ma, N. Peng, B. Yang, Influences of Fracturing Fluid Injection on Mechanical Integrity of Cement Sheath under Four Failure Modes, Energies. 11 (2018) 3534. https://doi.org/10.3390/en11123534.

[73] H. Xu, N. Peng, T. Ma, B. Yang, Investigation of Thermal Stress of Cement Sheath for Geothermal Wells during Fracturing, Energies. 11 (2018) 2581. https://doi.org/10.3390/en11102581.

[74] M. Bagheri, S.M. Shariatipour, E. Ganjian, A methodology for reactive transport modelling and geomechanical investigation of wellbores in CO2 storage sites, Constr. Build. Mater. (2020).

[75] I.B. Fridleifsson, R. Bertani, E. Huenges, J. Lund, A. Ragnarsson, L. Rybach, The possible role and contribution of geothermal energy to the mitigation of climate change, IPCC Scoping Meet. Renew. Energy Sources. (2008) 59–80. http://scholar.google.com/scholar?hl=en&btnG=Search&q=intitle:The+possible+role+and+contribution+of+geothermal+energy+to+the+mitigation+of+climate+change#0.

[76] I.M. Kutasov, L. V Eppelbaum, Wellbore and Formation Temperatures During Drilling, Cementing of Casing and Shut-in, World Geotherm. Congr. 2015. (2015) 19–25.

[77] E. Lindeberg, Modelling pressure and temperature profile in a CO2 injection well,

Energy Procedia. 4 (2011) 3935–3941. https://doi.org/10.1016/j.egypro.2011.02.332.

[78] G.Y. Gor, J.H. Prévost, Effect of CO2 injection temperature on caprock stability, Energy Procedia. 37 (2013) 3727–3732. https://doi.org/10.1016/j.egypro.2013.06.267.

[79] E.T. Brown, E. Hoek, Trends in relationships between measured in-situ stresses and depth, Int. J. Rock Mech. Min. Sci. 15 (1978) 211–215. https://doi.org/10.1016/0148-9062(78)91227-5.

[80] Z. Duan, R. Sun, An improved model calculating CO2 solubility in pure water and aqueous NaCl solutions from 273 to 533 K and from 0 to 2000 bar, Chem. Geol. 193 (2003) 257–271. https://doi.org/10.1016/S0009-2541(02)00263-2.

[81] C.I. Steefel, A.C. Lasaga, A coupled model for transport of multiple chemical species and kinetic precipitation/dissolution reactions with application to reactive flow in single phase hydrothermal systems, Am. J. Sci. 294 (1994) 529–592. https://doi.org/10.2475/ajs.294.5.529.

[82] C. Chang, M.D. Zoback, A. Khaksar, Empirical relations between rock strength and physical properties in sedimentary rocks, J. Pet. Sci. Eng. 51 (2006) 223–237. https://doi.org/10.1016/j.petrol.2006.01.003.

[83] P. Rochette, P. Labossiere, A Plasticity Approach for Concrete Columns Confined with Composite Materials, Adv. Compos. Mater. Bridg. Struct. -INTERNATIONAL Conf. (1996) 359–366. https://www.tib.eu/en/search/id/BLCP%3ACN018623351/A-Plasticity-Approach-for-Concrete-Columns-Confined/#documentinfo (accessed January 22, 2019).

[84] R. Chamrova, Modelling and Measurement of Elastic Properties of Hydrating Cement Paste, 2010.

[85] H.M. Jennings, J.J. Thomas, J.S. Gevrenov, G. Constantinides, F.J. Ulm, A multi-technique investigation of the nanoporosity of cement paste, Cem. Concr. Res. 37 (2007) 329–336. https://doi.org/10.1016/j.cemconres.2006.03.021.

[86] G. Constantinides, F.J. Ulm, The nanogranular nature of C-S-H, J. Mech. Phys. Solids. 55 (2007) 64–90. https://doi.org/10.1016/j.jmps.2006.06.003.

[87] G. Constantinides, F.J. Ulm, The effect of two types of C-S-H on the elasticity of cement-based materials: Results from nanoindentation and micromechanical modeling, Cem. Concr. Res. 34 (2004) 67–80. https://doi.org/10.1016/S0008-8846(03)00230-8.

[88] C. Merkel, J. Deuschle, E. Griesshaber, S. Enders, E. Steinhauser, R. Hochleitner, U. Brand, W.W. Schmahl, Mechanical properties of modern calcite- (Mergerlia truncata) and phosphate-shelled brachiopods (Discradisca stella and Lingula anatina) determined by nanoindentation, J. Struct. Biol. 168 (2009) 396–408. https://doi.org/10.1016/J.JSB.2009.08.014.

[89] M.A. Hopcroft, W.D. Nix, T.W. Kenny, What is the Young's Modulus of Silicon?, J. MICROELECTROMECHANICAL Syst. 19 (2010). https://doi.org/10.1109/JMEMS.2009.2039697.

[90] M. Moner-Girona, A. Roig, E. Molins, E. Martínez, J. Esteve, Micromechanical

properties of silica aerogels, Appl. Phys. Lett. 75 (1999) 653–655. https://doi.org/10.1063/1.124471.

[91] W. Liang, C. Zhang, H. Gao, X. Yang, S. Xu, Y. Zhao, Experiments on mechanical properties of salt rocks under cyclic loading, J. Rock Mech. Geotech. Eng. 4 (2013) 54–61. https://doi.org/10.3724/sp.j.1235.2012.00054.

[92] S. Harsh, Z. Shen, D. Darwin, Strain-rate sensitive behavior of cement paste and mortar in compression, ACI Mater. J. 87 (1990) 508–516. https://doi.org/10.14359/1931.

[93] K. Velez, S. Maximilien, D. Damidot, G. Fantozzi, F. Sorrentino, Determination by nanoindentation of elastic modulus and hardness of pure constituents of Portland cement clinker, Cem. Concr. Res. 31 (2001) 555–561. https://doi.org/10.1016/S0008-8846(00)00505-6.

[94] X. Wang, K. V. Subramaniam, Ultrasonic monitoring of capillary porosity and elastic properties in hydrating cement paste, Cem. Concr. Compos. 33 (2011) 389–401. https://doi.org/10.1016/J.CEMCONCOMP.2010.11.001.

[95] Z. Zhang, H. Wang, Effect of thermal expansion annulus pressure on cement sheath mechanical integrity in HPHT gas wells, Appl. Therm. Eng. 118 (2017) 600–611. https://doi.org/10.1016/j.applthermaleng.2017.02.075.

[96] Z.H. Shui, R. Zhang, W. Chen, D.X. Xuan, Effects of mineral admixtures on the thermal expansion properties of hardened cement paste, Constr. Build. Mater. 24 (2010) 1761–1767. https://doi.org/10.1016/j.conbuildmat.2010.02.012.

[97] M. Steiger, A.E. Charola, K. Sterflinger, Weathering and Deterioration, in: Stone Archit., 4th ed., Springer-Verlag Berlin Heidelberg, 2011: pp. 227–316. https://doi.org/10.1007/978-3-662-10070-7.

[98] K.K. Phani, S.K. Niyogi, Young's modulus of porous brittle solids, J. Mater. Sci. 22 (1987) 257–263. https://doi.org/10.1007/BF01160581.

[99] Z. Lafhaj, M. Goueygou, A. Djerbi, M. Kaczmarek, Correlation between porosity, permeability and ultrasonic parameters of mortar with variable water / cement ratio and water content, Cem. Concr. Res. 36 (2006) 625–633. https://doi.org/10.1016/j.cemconres.2005.11.009.

[100] Y.X. Li, Y.M. Chen, J.X. Wei, X.Y. He, H.T. Zhang, W.S. Zhang, A study on the relationship between porosity of the cement paste with mineral additives and compressive strength of mortar based on this paste, Cem. Concr. Res. 36 (2006) 1740–1743. https://doi.org/10.1016/j.cemconres.2004.07.007.